University of Alberta

Synthesis of Al-Ni Based HTlcs Using Urea Coprecipitation and an Investigation into the Coprecipitation Mechanism

by

Bo Lu

A thesis submitted to the Faculty of Graduate Studies and Research in partial fulfillment of the

requirements for the degree of Master of Science

in

Chemical Engineering

Department of Chemical and Materials Engineering

Edmonton, Alberta

Spring 2006

Library and Archives Canada

Published Heritage Branch

395 Wellington Street
Ottawa ON K1A 0N4
Canada

Bibliothèque et Archives Canada

Direction du Patrimoine de l'édition

395, rue Wellington
Ottawa ON K1A 0N4
Canada

Your file Votre référence
ISBN: 0-494-13846-7
Our file Notre référence
ISBN: 0-494-13846-7

NOTICE:
The author has granted a non-exclusive license allowing Library and Archives Canada to reproduce, publish, archive, preserve, conserve, communicate to the public by telecommunication or on the Internet, loan, distribute and sell theses worldwide, for commercial or non-commercial purposes, in microform, paper, electronic and/or any other formats.

The author retains copyright ownership and moral rights in this thesis. Neither the thesis nor substantial extracts from it may be printed or otherwise reproduced without the author's permission.

AVIS:
L'auteur a accordé une licence non exclusive permettant à la Bibliothèque et Archives Canada de reproduire, publier, archiver, sauvegarder, conserver, transmettre au public par télécommunication ou par l'Internet, prêter, distribuer et vendre des thèses partout dans le monde, à des fins commerciales ou autres, sur support microforme, papier, électronique et/ou autres formats.

L'auteur conserve la propriété du droit d'auteur et des droits moraux qui protège cette thèse. Ni la thèse ni des extraits substantiels de celle-ci ne doivent être imprimés ou autrement reproduits sans son autorisation.

In compliance with the Canadian Privacy Act some supporting forms may have been removed from this thesis.

While these forms may be included in the document page count, their removal does not represent any loss of content from the thesis.

Conformément à la loi canadienne sur la protection de la vie privée, quelques formulaires secondaires ont été enlevés de cette thèse.

Bien que ces formulaires aient inclus dans la pagination, il n'y aura aucun contenu manquant.

Canada

Abstract

Nickel-aluminum based hydrotalcite-like compounds (HTlcs) doped with 2 wt % copper were synthesized by coprecipitation using a urea hydrolysis method. The average size of the coprecipitated particles ranged from 4 nm to 15 nm. The particles displayed a certain degree of coagulation and edge-surface platelet interactions. The effects of several parameters on the composition, physical morphology, average particle size and particle size distribution of the precipitates were systematically studied. Particle growth was found to be the reason for the relatively large size particle formed in low urea concentration environments, while agglomeration was believed to be responsible for large particle size in high urea concentration environments.

The bulk pH curve of the coprecipitation process shows two distinct buffer regions. The first pH buffer region is considered to be controlled by the reaction of OH^- with trivalent metal ions while the second pH buffer region, controlled by the reaction with divalent metal ions. When multiple divalent metals were present in the bulk solution, more buffer region may occur according to the coprecipitation properties of the divalent metals. From X-ray Diffraction (XRD) characterization and degree of coprecipitation determined by Atomic Absorption Spectroscopy (AAS), the formation of an aluminum hydro-complex, $Al(OH)_{3n-1}(H_2O)_m^+$, is proved by to be a possible intermediate before HTlc precipitates. A new tentative coprecipitation scheme in an Al-Ni-Cu system was derived from this study. The effect of pretreatment conditions of the precipitated HTlcs, inclusion of sodium ions and doping of copper on catalyst properties is also discussed.

Acknowledgement

I would like to acknowledge the great contributions of my two supervisors: Dr. Zhenghe Xu and Dr. Thomas H. Etsell for their superior supervision and guidance during the past years of my study. I would also like to thank Dr. Reza A. Naghash for valuable discussion and suggestions.

Special thanks are also given to the whole Coal group: Dr. Clark Lu, Dr. David Kelly, Dr. Jaewon Choung, Ms. Janet Dong, Ms. Yan Liu, Ms. Nan Lu, et al. Thanks are also due to Ms. Tina Barker, Mr. Shiraz Merali and Dr. Diane Caird (Department of Earth & Atmospheric Sciences) for kindly help on TEM, SEM, XRD scanning and AAS tests.

I also acknowledge the research funding from NSERC/EPCOR/AERI Industrial Research Funding and COURSE program.

Contents

List of Figures

1 Introduction 1

1.1 Composition and Structure of Hydrotalcite-like Compounds 1

1.2 Applications of HTlcs 3

1.2.1 Possible Applications of HTlcs 3

1.2.2 Production of Hydrogen and Nano-carbon Tubes 4

1.3 Synthesis Methods 6

1.3.1 Normal Methods 6

1.3.2 Urea Coprecipitation Method 9

1.4 Coprecipitation Reaction Schemes 10

1.5 Pretreatment of the Coprecipitated HTlc Particles: Catalyst Formation 12

1.6 Activity of the Catalyst: A Final Product from the Coprecipitated HTlc Particles after Calcinations and Reduction 13

1.6.1 Effect of Sodium 14

1.6.2 The Effect of Doping Copper 15

2 Experimental methods 18

2.1 Sample Preparation 18

2.1.1 Constant pH Titration 18

2.1.2 Increasing pH Titration 19

2.1.3 Increasing pH bulk coprecipitation Using Urea 20

2.2 Characterization Methods 21

2.3 Conversion Test 23

3 Results and Discussion 25

3.1 General Results 25

3.1.1 Coprecipitated HTlc Particles: Effects of Coprecipitation Parameters 25

3.1.2 Coprecipitation Reaction Scheme 28

3.2 Effect of Coprecipitation Parameters on Particle Size and Morphology 29
3.2.1 Effect of PTR 29
3.2.2 Effect of Reaction Time 39
3.2.3 Effect of Reaction Temperature 46
3.3 Coprecipitation Chemistry 48
3.3.1 Different Stages of Coprecipitation Process 48
3.3.2 Precipitation Sequence 52
3.3.3 Possible Intermediates 55
3.3.4 Reaction Scheme 62
3.4 Formation of Nano-carbon Tubes 67

4 Conclusions 71

5 Suggestions for Future Work 74

Nomenclature 75

References 76

List of Figures

Figure 1.1	Structure of $Mg_{1-x}Al_x(OH)_2 \cdot x/2\ CO_3 \cdot 4H_2O$.	2
Figure 1.2	Specific activity as a function of sodium content in the catalysts.	14
Figure 1.3	Methane conversion as a function of copper content in the catalyst precursor.	16
Figure 2.1	Titration equipment set.	19
Figure 2.2	Coprecipitation equipment set.	20
Figure 2.3	The equipment used to characterize the catalytic activity of the catalyst.	24
Figure 3.1	SEM micrograph of HTlc particles prepared by urea hydrolysis coprecipitation.	25
Figure 3.2	SEM micrograph of HTlc particles prepared by coprecipitation. PTR = 3.0, TMC = 0.4 mol/L, t = 24h, T = 99℃. Samples were washed thoroughly with water after filtration and centrifugation.	27
Figure 3.3	SEM micrograph: HTlc particles prepared by coprecipitation. PTR = 9.0, TMC = 0.4 mol/L, t = 24h, T = 99℃. Samples were washed thoroughly with water after filtration and centrifugation.	27
Figure 3.4	Bulk pH curves under different PTR values.	30
Figure 3.5	The reciprocal of the time needed to reach a bulk pH of 4.5 at different PTR values.	31
Figure 3.6	The reciprocal of the time needed to reach a bulk pH of 6.5 at different PTR values.	31
Figure 3.7	Average particle size as a function of PTR, with t = 6 h, TMC = 0.4 mol/L, reaction temperature = 99 ℃.	32
Figure 3.8	Average particle size as a function of PTR, with t = 24 h, TMC = 0.4 mol/L, reaction temperature = 99 ℃.	33
Figure 3.9-12	SEM micrograph of HTlc particles precipitated by urea hydrolysis under different conditions. Samples were washed thoroughly with water and acetone after filtration and centrifugation.	35
Figure 3.13	XRD patterns of samples prepared under different PTR, with t = 24h, T = 99℃ and TMC = 0.2 mol/L.	38

Figure 3.14 XRD patterns of samples prepared under different PTR, with t = 6h, T = 99℃ and TMC = 0.2 mol/L. 39

Figure 3.15 Average particle size of precipitates sampled at different reaction time, with T = 99℃, TMC = 0.2 mol/L and PTR = 3.0. 40

Figure 3.16 Average particle size of precipitates synthesized under different PTR with T = 99℃ and TMC = 0.2 mol/L. Also a comparison between the samples picked at t = 6h and t = 24h. 41

Figure 3.17*4 SEM micrograph of particles precipitated under different conditions. 42

Figure 3.18 XRD patterns of samples picked at t = 6 h and t = 24 h, under reaction conditions of PTR = 3.0, TMC = 0.2 mol/L, T = 99 ℃. 44

Figure 3.19 XRD patterns of samples picked at t = 6 h and t = 24 h, under reaction conditions of PTR = 9.0, TMC = 0.2 mol/L, T = 99 ℃. 45

Figure 3.20 Average particle size (um) as a function of bulk pH value. All the pH values are measured at 99 ℃. 45

Figure 3.21 Bulk pH curves under different reaction temperatures. TMC = 0.2 mol/L, PTR = 4.0. 47

Figure 3.22 Bulk pH curve with clear two buffer regions. Ni-Cu-Al coprecipitation, PTR = 1.0, T = 99 ℃, TMC = 0.2 mol/L. 48

Figure 3.23 Accelerated reaction with PTR = 4.0, TMC = 0.2 mol/L and T = 99 ℃. 49

Figure 3.24 Bulk pH curves of comparison tests between Al-Ni system (25% Al + 75% Ni) and Fe-Ni system (25% Fe + 75% Ni) with PTR = 4.0, TMC = 0.2 mol/L and T = 99 ℃. 50

Figure 3.25 Bulk pH curves of comparison tests among Al-Ca, Al-Ni and Al-Cu systems. Titration of 3:1 $[M^{2+}]/[M^{3+}]$ solutions with TMC = 0.2 mol/L and T = 85 ℃. 51

Figure 3.26 Bulk pH curves of titration test by Na_2CO_3 addition at room temperature and under vigorous stirring. 52

Figure 3.27 AAS results to investigate the precipitation sequence. The mole ratios of Ni: Cu and divalent metal: trivalent metal were examined in a Ni-Cu-Al system. Coprecipitation was performed at T = 99 ℃, PTR = 4.0 and TMC = 0.2 mol/L. 53

Figure 3.28 Concentration of nickel and copper in the liquid phase with increasing amount of Na_2CO_3 addition. Titration test at T = 95 ℃, V = 200 mL, TMC = 0.2 mol/L and Ni: Al: Cu = 2:1:1 (mole ratio), titrated by 0.25 mol/L Na_2CO_3. 55

Figure 3.29 Concentration of aluminum in the liquid phase vs. amount of Na_2CO_3 added to the solution. Titration test at T = 95 ℃. V = 100 mL, TMC = 0.2 mol/L, 73% nickel nitrate, 25% aluminum nitrate and 2% copper nitrate, titrated by 0.1 mol/L Na_2CO_3. 57

Figure 3.30 Concentration of aluminum in the liquid phase as a function of bulk pH value. 58

Figure 3.31 XRD samples were taken and prepared for XRD tests at the light points. Coprecipitation using urea with T = 99 ℃, TMC = 0.2 mol/L and PTR = 4.0. 60

Figure 3.32 XRD patterns of samples at different stages of the coprecipitation process (from sample #1 picked at bulk pH = 5.10 to sample #5 picked at bulk pH = 6.50). 61

Figure 3.33 XRD pattern. $Al(OH)_{3(solid)}$ + $Ni(NO_3)_2$, PTR = 4.0, T = 96℃, t = 3.0 h. 64

Figure 3.34 Aluminum hydro-complex colloid. Coprecipitation with T = 99 ℃, PTR = 4.0 and TMC = 0.2 mol/L. 66

Figure 3.35 TEM micrograph of the nano-carbon tubes formed by decomposing methane. The coprecipitated HTlc catalyst precursor with 75% Ni, 25% Al and 2% Cu was calcined and reduced before used as the final catalyst. 68

Figure 3.36 TEM micrograph of another part of the nano-carbon tubes formed by decomposing methane. Clumps of catalysts (black dots) can be seen in this picture. 70

1 Introduction

1.1 Composition and Structure of Hydrotalcite-like Compounds

Hydrotalcite, which is discovered in Sweden around 1842, is a hydroxycarbonate of magnesium and aluminium that usually occurs in the form of foliated and contorted plates and fibrous masses. Other mixed hydroxycarbonate containing different divalent and trivalent metals were discovered later on to have similar structure as hydrotalcite. However, not much attention was given to the synthesis of hydrotalcite and hydrotalcite-like compounds until in 1970, when the first patent appeared and referred to a hydrotalcite-like structure as an optimal precursor for the preparation of hydrogenation catalysts [1].

Hydrotalcite-like compounds (HTlcs), which are also known as layered double hydroxides (LDHs) and Feitknecht compounds (FCs), are a family of natural and synthetic materials of the general type $(M(II)_{1-a} M(III)_a (OH)_a) (X_{a/2}) \cdot y\, H_2O$, where X is, for example, CO_3^{2-}. They are structurally similar to the mineral brucite with a fraction of M(II) ions replaced by M(III) ions. This replacement results in a net positive charge on the octahedral layers, which is balanced by exchangeable interlayer ions lying in the interlayer region between the two brucite-like sheets. Crystalline water also exists in the free space of this interlayer. In a typical carbonate HTlc, the CO_3^{2-} groups and H_2O could be eliminated without destroying the crystallinity of the HTlc particles as the CO_3^{2-} groups are situated flat in the interlayer and H_2O is loosely bound.[1] The crystal structure of an Mg-Al based HTlc is shown in Figure 1.1.

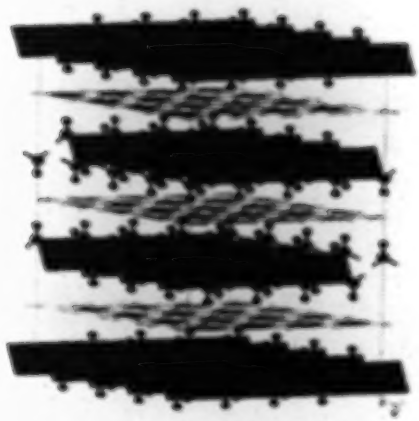

Figure 1.1 Structure of $Mg_{1-x}Al_x(OH)_2 \cdot x/2\ CO_3 \cdot 4H_2O$ [2]

Most M(II) can be accommodated in the space of the close packed configuration of OH groups in brucite-like layers, with except of Be^{2+}, which is too small for octahedral coordination, and Ba^{2+}, which is considered to be too big for the holes in the brucite-like layers. Whether the presence of trace Cd^{2+} can form HTlc is still under discussion. Among all the divalent metals from Mg^{2+} to Mn^{2+}, a special attention should be paid to Cu^{2+} because of its abnormal coprecipitation properties. Cu^{2+} cannot form HTlc unless another divalent cation is present [1]. All the trivalent ions, except V^{3+} and Ti^{3+} (not stable in air), with atomic radii raging from 0.5 to 0.8 Å, are capable of forming HTlcs [1].

As for the anions, there is practically no limitation to the nature of anions which can form HTlcs. Inorganic anions (e.g. Cl^-, Br^-, I^-, OH^-, CO_3^{2-}, SO_4^{2-}), heteropolyacids (e.g. $PMo_{12}O_{40}^{3-}$, $PW_{12}O_{40}^{3-}$), organic acids (e.g. adipic, oxalic, succinic) and layered compounds (e.g. $[Mg_3(OH)_2Si_3AlO_{10}]^-$) were all found to be able to form HTlcs. However, the high affinity of CO_3^{2-} for HTlc could bring problems when high purity

HTlc containing other anions different from carbonate is desired. It could be very difficult to avoid contamination from the CO_2 present in the aqueous solution [1].

1.2 Applications of HTlcs

1.2.1 Possible Applications of HTlcs

One of the main advantages of HTlc is that the cations have a uniform distribution in the brucite-like layers. During the coprecipitation process, which is the most popular method to prepare HTlcs [1], a high degree of crystallinity was formed. Due to the slow solid phase diffusion of metal ions during calcination, the crystalline structure maintains and HTlc precursor results in a well-mixed oxide phase even after calcination, which is ideal for making a catalyst.

The Ni-Al based HTlc has been proved to be a good precursor for a low temperature (around 800K) catalyst to grow carbon fibers. The Ni-Al based HTlc, after calcination and reduction, would result in a defective and active nickel phase mixed with the irreducible part, in this case, Al_2O_3. The irreducible part provides support for the active nickel particles and, from some researchers' point of view, even enhances the activity of the catalyst [3].

The calcinated HTlcs are also used in the field of heterogeneous catalysis because of its high surface area and formation of stable homogeneous mixture of oxides with small particle size. Moreover, the "memory effect" to reconstruct of the original hydrotalcite structure when contacting the product with aqueous solutions containing

various anions enables HTlc products to find their place in applications such as the scavenging of chlorine ions and the water purification [1].

1.2.2 Production of Hydrogen and Nano-carbon Tubes

Hydrogen is playing an increasingly important role and large volumes have been used in chemical, food and refining industries. Stringent environmental regulations and recent advances in fuel cells have further promoted the exploration for effectively producing pure hydrogen.

Electrolysis and photo-catalytic decomposition of water are the most direct ways to produce pure hydrogen. However, the former method was not regarded as economically practical while the latter encountered technical difficulties. Dry reforming and steam reforming of methane and other hydrocarbon feedstock once were the most popular and economical technology for the production of hydrogen. Andrews, Armor and Steinberg [4-6] have several publications on steam reforming of methane (SRM). However, this route introduces CO_2 along with the production of hydrogen. Furthermore, one of the products of steam reforming is CO, which is capable of poisoning the electro-catalyst in fuel cells even with a concentration as low as a few ppm. CO removal processes, such as converting CO in synthesis gas using the water-gas shift reaction are inadequate to prevent this CO poisoning. Although a reverse methanation reaction which could help reduce the CO concentration to the sub-ppm level was later proposed to minimize the negative influence of CO, a strong need to develop a CO-free process for hydrogen generation persists, driven by economical considerations and environmental protection.

An alternative route for hydrogen production is to crack hydrocarbons directly into hydrogen and carbon. Formation of CO_2 and CO could be avoided in this case and the subsequent steps for the removal of CO are not needed. Although this route was reported to be superior to steam reforming from both economical and energy efficiency points of view [6, 7], the relatively high temperature required for decomposition is still a drawback.

CO-free methane decomposition processes, using non-oxidative catalysts were proposed as an alternate source for producing pure hydrogen. Muradov [8, 9] has attempted catalytic pyrolysis of methane to produce CO_2-free and CO-free hydrogen using alumina supported Fe_2O_3 and NiO (10 wt %) at 850 ℃ and has reached an 11 volume% methane conversion. Another possible approach was published by Bromberg et al. [10-12] who tried to use plasma as a heat source to produce hydrogen in a fuel converter for internal combustion engines. Solar energy has also been used as the heat source for thermal dissociation of methane to hydrogen and carbon black [13]. The research has been extended to different feed gas compositions using a great variety of catalysts with different nickel content [14-24]. Copper was later found to be able to increase both the temperature of maximum conversion and the maximum conversion percentage when doped into the nickel-based catalyst [18]. Methane conversion up to 45% has been achieved under 550 ℃ with 10 wt% Ni on SiO_2, H-ZSM-5 or HY supports as the catalyst [20]. This route also produces filamentary nano-carbon tubes. However, a drawback of this route is that the catalyst was proved deactivated due to the spatial limitations imposed on these long cylindrical hollow filaments with a Ni particle at the tip of each individual filament.

Recent years have also seen an increasing interest in the nano-carbon materials. Nano-carbon tubes and nano-carbon fibers, due to their excellent properties and potential utilization, have been paid considerable attention. The main techniques that have been used to produce nano-carbons are the arc-discharge evaporation of graphite with a metal catalyst [25-27] and the catalytic growth of carbon fibers at low temperature from decomposition of hydrocarbons or disproportionation of carbon monoxide [28-32]. Although attractive to produce single and multi-walled nano-carbon tubes by the arc-discharge evaporation technique, it is difficult to scale up and requires relatively high temperature and thus becomes quite energy intensive.

The nano-carbon tubes produced by catalytic growth, especially when HTlc particles were used as the catalyst precursor, show a curved hollow tubular structure with many dislocations or flaws. According to some recent reports [33, 34] these nano-carbon tubes have a myriad of applications such as storage of hydrogen and many other gases, catalyst supports, the tip for scanning probe microscopy and absorbent of hydrocarbons.

1.3 Synthesis Methods

1.3.1 Normal Methods

Coprecipitation has been recognized as the most popular method for preparing HTlcs. Several synthesis methods have been reported by early researcher to make HTlc particles. As well known, it is necessary to reach supersaturation conditions to cause

coprecipitation of two or more cations. Both evaporation and variation of bulk pH have been used to reach such supersaturation conditions.

The four main coprecipitation methods that have been used to synthesize HTlc particles are:

1) Titration with NaOH and/or $NaHCO_3$ in an increasing bulk pH environment. The first synthetic HTlc was prepared by titration of very dilute solutions of Mg^{2+} and Al^{3+} with a dilute caustic solution up to pH 10. The flocculated precipitate was then placed in a dialysis bag and immersed in water at 333K for one month, during which chlorine and sodium ions were supposed to be removed and CO_2 was taken from the atmosphere into the precipitates. Crystalline particles were obtained at the end of the prolonged dialysis stage [1].

The titration curves published by early researchers show that several buffer regions occur during the coprecipitation and a sequential precipitation of ions may exist. However, simple sequential precipitation definitely does not occur. It is noticed that the precipitation pH of Mg in a Mg-Al system could be much lower than the precipitation pH of $Mg(OH)_2$, and similar effects in Cu-Zn-Al system and Ni-Al system have also been reported. These effects indicate the occurrence of coprecipitation in these systems, in which different metal cations may affect each other. In some cases, precipitation sequence may exist among the different divalent metals.

2) Titration with NaOH and/or $NaHCO_3$ in a constant bulk pH environment (low supersaturation coprecipitation). This method is the most frequently used method in the preparation of HTlcs in the 1990s. In this method, a diluted metal salts solution and base solution were added slowly into the reactor to reach a low supersaturation condition. The bulk pH is controlled through the speed of addition of the two diluted solutions. The conditions that most commonly used are: pH ranging from 7 to 10, reaction temperature from 333 to 353K, low concentration of reagents and low flow of the two streams [1].

The low supersaturation conditions encourage particle growth instead of nucleation. Precipitates with higher crystallinity and larger particle size tend to form in the low supersaturation conditions, compared to that formed in high supersaturation conditions where the rate of nucleation can be much higher than the rate of particle growth.

3) Rapid addition of the metal salts solution into the base solution (high supersaturation coprecipitation). The bulk pH is again held constant through out the whole reaction. The high supersaturation coprecipitation usually gives rise to less crystalline precipitates with generally smaller size. This is because nucleation is the dominant reaction in high supersaturation coprecipitation process. Amorphous precipitates instead of any crystalline HTlc were also reported to be formed under extremely high supersaturation conditions. However, nucleates will normally tend to agglomerate and form large clumps (micron size).

It is also reported that the Cu-Zn-Al catalysts prepared by this method had surface areas slightly higher than those for the same compositions prepared at low supersaturation conditions while all other features were similar. This is suspected to be the result of the lower degree of crystallization of the precipitates.

Except for the above three traditional methods, the 4th coprecipitation method is the urea coprecipitation method.

1.3.2 Urea Coprecipitation Method

Although HTlc precursors are generally prepared by the constant pH coprecipitation methods, an apparent disadvantage is that residual sodium in the coprecipitated HTlc precursors greatly reduces the activity of the catalyst. It has been reported that 0.5 wt% sodium would be enough to make the catalyst inactive [35]. Thus, for better catalytic performance, it is mandatory to use sodium-free catalyst precursors. Using urea as the source of OH^- and CO_3^{2-} can effectively eliminate the inactivation pollution from residual sodium. In the urea coprecipitation method, solid urea was added into the metal salts solution and heated up to a certain temperature [1]. The hydrolysis of urea liberates the anions needed for the coprecipitation and results in an increasing pH environment.

The most significant practical advantage of employing the urea hydrolysis method is the ease in obtaining guaranteed sodium-free precipitates instead of relying on an intricate washing process required by the normal constant pH methods.

Another remarkable advantage of the urea hydrolysis method is that urea hydrolysis progresses slowly and leads to a low degree of supersaturation during coprecipitation. This low supersaturation condition would help minimize the overlapping of particle growth and nucleation of new particles, and thus develop mono-dispersed particles. People have used this method for the synthesis of well crystallized Li-Al, Mg-Al, Zn-Al and Ni-Al based HTlcs [36-39].

Except for the concern for sodium free HTlcs, several requirements have to be met to obtain a pure HTlc. Correct ratios among different metal cations and the ratio between the metal cations and anions have to be kept throughout the coprecipitation process. These ratios include:

$$0.2 \leq M(III) / [M(II) + M(III)] \leq 0.4$$

$$1/n \leq A^{n-} / M(III) \leq 1.0$$

As for the coprecipitation conditions, although no strict requirements exist on these conditions, a number of parameters, or factors, may affect the quality of the catalyst. These parameters include the composition of the precursor, the coprecipitation temperature and time, the type of reagents, the washing method, the calcination temperature, the composition of the reduction activation gas, and also the reduction activation temperature and time. Any of these parameters has direct or indirect influence on either the physical structure or chemical composition of the catalyst particles, and thus affect the catalyst's activity.

1.4 Coprecipitation Reaction Schemes

Several possible coprecipitation reaction schemes have been proposed by earlier researchers. Boclair and Braterman [40] thought that the formation of the trivalent metal hydroxide exists in coherence with the first buffer region of the coprecipitation reaction. They suggested that the pH of this buffer region should depend only on the activity and identity of the trivalent metal being used and is independent of the specific divalent metals. The main equilibrium reaction at this stage of the reaction could be described as:

$$M(III)^{3+}_{(aq)} + 3OH^-_{(aq)} \leftrightarrow M(III)(OH)_3 \qquad (1.1)$$

In the following stage of the reaction, in which another buffer region with a higher bulk pH value is reached, Boclair and Braterman [40] think that the trivalent metal would have been fully precipitated as $M(III)(OH)_3$. As for the second stage of the reaction, another equation was suggested as follows:

$$M(III)(OH)_3 + 2M(II)^{2+}_{(aq)} + 3OH^- + Cl^- \leftrightarrow M(III)[M(II)]_2(OH)_6Cl \text{ (HTlc)} \qquad (1.2)$$

They noticed that equilibrium in the second buffer region is much slower than that in the first buffer region, and suggested that this is because the second reaction involves a solid reactant, $M(III)(OH)_3$ [40].

Another reaction scheme was reported by Adachi-Pagno and his co-workers four years later [41]. They discussed the intermediate that may exist before HTlc particles were precipitated. Instead of supporting the direct formation of solid $M(III)(OH)_3$,

Adachi-Pagno and his co-workers suggested that a more complicated "aluminum aquo hydroxo complex" would form before the precipitation of $Al(OH)_3$ took place in the Mg-Al system. In the second buffer region, it was postulated that Mg^{2+} would incorporate into the solid hydroxide probably under a dissolution/precipitation mechanism [41].

Recently, Rao et al. proposed another new reaction scheme [42]. They listed three reactions that explain what happened during the coprecipitation process of the Mg-Al system. The three reactions can be written as:

$$Mg(H_2O)_n^{2+} + H_2O \rightarrow Mg(OH)(H_2O)_{n-1}^{+} + H_3O^{+} \quad (1.3)$$

$$Al(H_2O)_n^{3+} + H_2O \rightarrow Al(OH)(H_2O)_{n-1}^{2+} + H_3O^{+} \quad (1.4)$$

$$Mg(OH)(H_2O)_{n-1}^{+} + Al(OH)(H_2O)_{n-1}^{2+} + OH^{-} + CO_3^{2-} \rightarrow MgAl(OH)_3CO_3 \cdot H_2O \quad (1.5)$$

1.5 Pretreatment of the Coprecipitated HTlc Particles: Catalyst Formation

Several pretreatment steps including calcination and reduction are needed to transform the HTlc precursors into catalysts. Since pretreatment of the coprecipitated nickel-alumina crystallites governs the activity and stability of the final catalysts, it is regarded as a very important step in preparation for the catalysts. There have been a number of studies to examine pretreatment variables such as calcination and reduction temperature.

Shephard [43] has reported data for the variation of total and nickel surface areas as a function of calcination temperature, and found that the total area decreased with increasing calcination temperature, particularly above 773K, and that the nickel surface area similarly decreased. Dzis'ko et al. [44] found that the nickel surface areas of the samples increased with increasing temperature of reduction for low nickel content catalysts, and nickel surface area would increase with nickel content. Borisova et al. [45] provided data showing that the nickel surface area would increase with nickel content at lower reduction temperatures, but decreases above a nickel content of 70%, which might be the result of sintering of the nickel crystallites. The relationship between surface areas and nickel contents was also reported by Iosht et al. [46] before Alzamora et al. [47] performed a systematic analysis of the effects of the anion in the original precipitate, the calcination temperature and the reduction temperature on total and nickel surface areas. CO_3^{2-} was found capable to give larger surface areas than NO_3^- and Cl^-, while the temperature of calcination had a negative effect on both the total surface area and the nickel surface area, i. e., surface area decreased as calcination temperature was increased. The nickel surface was further found to increase with reduction temperature below a certain temperature limit, and then started to decrease when reduction temperature went beyond that limit [47].

1.6 Activity of the Catalyst: A Final Product from the Coprecipitated HTlc Particles after Calcinations and Reduction

This section deals with the catalytic behavior of the catalysts whose precursors were the HTlc particles already discussed. The coprecipitated HTlc particles were normally calcined at 475℃ for 12 hours and reduced in hydrogen at 650℃ for 6 hours to

transform them into the final catalysts. The catalysts prepared by HTlc decomposition should have the following attributes: 1) higher activity, 2) higher stability and lifetime, 3) absence of alkali metals [1]. However, the coprecipitated HTlc particles prepared by traditional methods need to be washed thoroughly to remove the residue sodium and doped with copper to ensure these beneficial properties. The effects of residual sodium and doping of in the catalysts are discussed in this section.

1.6.1 Effect of Sodium

It has been reported by Kruissink et al. [35] that the presence of sodium would greatly reduce the activity of coprecipitated nickel-aluminum catalysts. They carried out systematic research to study the effect of sodium on the catalyst's activity. The result is shown in Figure 3.37, in which a remarkable drop is observed when the sodium content in the coprecipitated nickel-aluminum catalyst increases from 0 to 1 wt %.

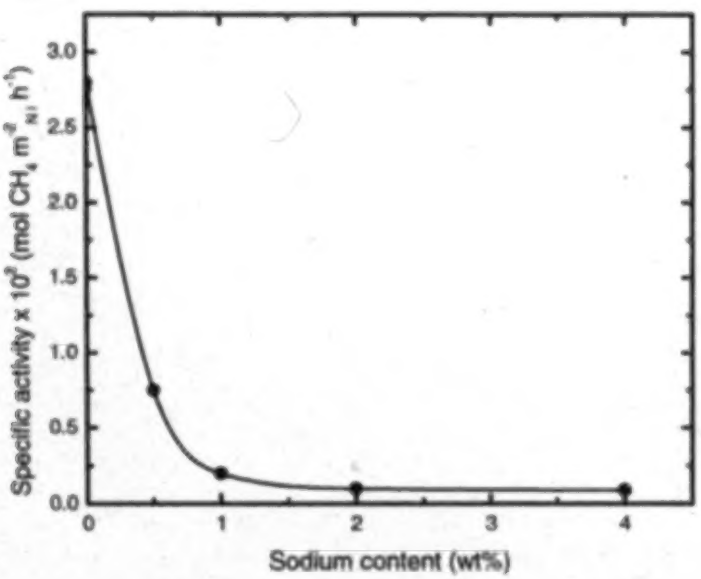

Figure 1.2 Specific activity as a function of sodium content in the catalysts. [35]

Huang and Richardson [48] reported a promoting effect on the catalytic activity when the sodium content was lower than 0.3 wt %, followed by a sharp drop in the catalyst's catalytic activity when the sodium content went higher. In our experiments this limit was not observed. However, the negative effect of sodium on the catalytic activity of the coprecipitated nickel-aluminum catalyst was confirmed.

Unwashed coprecipitated samples completely lost their catalytic activity while those washed with water only once showed very low catalytic activity. Only when the samples were washed three times or more, they were found to be reasonably reactive.

1.6.2 The Effect of Doping Copper

Although carbon formation on transition metal catalysts from decomposition of hydrocarbons has been extensively studied for many years, substantial operational problems still exist in a number of industrial catalytic processes. One of them is the accumulation of huge amounts of carbon in and on the catalyst pellets, which can create severe problems in the reactors.

One way suggested to reduce the risk of carbon fiber blockage is to add an agent to the surface of the catalysts, which partially poisons the carbon formation reaction. Sulfur has been chosen as the selective poisoning agent in industrial steam reforming, and adding copper to the catalyst surface is another way to achieve the same effect in hydrocarbon decomposition reactions.

Copper is a unique divalent metal in the case of forming HTlc particles as it cannot form HTlc unless another divalent metal is present. Furthermore, the copper content should not be higher than 50% (in all the divalent metals). Otherwise the copper compound would form distorted octahedra [1]. However, this deviant behavior of Cu^{2+} in comparison with other divalent metal cations does not prevent it from becoming a good "third component" when in an appropriate amount.

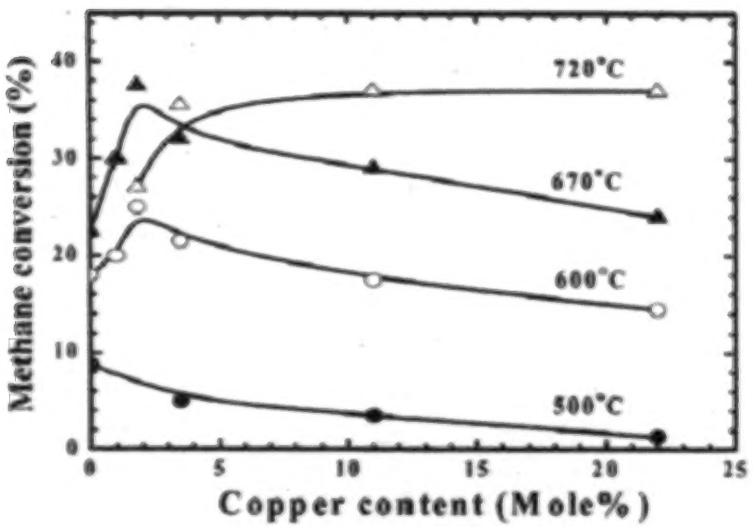

Figure 1.3 Methane conversion as a function of copper content in the catalyst precursor. [49]

Normally, the conversion reaction temperature has a strong effect on the deactivation rate of the catalyst and thus affects the amount of nano-carbon tubes produced by decomposing methane. The addition of copper greatly weakens the requirement of the reaction temperature for nano-carbon tube formation. It was reported that the addition of Cu (up to 25 wt %) to the catalyst increased both the temperature of maximum conversion and the maximum conversion percentage (Figure 3.38). These help to promote the production of nano-carbon tubes. Furthermore, doping copper in the

mixture of oxides would help remove both the amorphous carbon and inert graphite that may form on the surface of nickel, thus improving the catalytic activity. In our experiments, the samples with 2% copper sustained remarkably longer activity before the accumulation of carbon caused a sharp increase in the pressure inside the reactor. While the conversion ratio roughly remained constant, the total amount of nano-carbon tubes produced increased when 2% copper doped catalysts was used as the reaction time could be extended. However, too much copper would decrease the catalytic activity, since copper is not as effective a catalyst as nickel in the methane decomposition process.

Changes in the structure of the catalyst after the introduction of a certain amount of copper have also attracted researchers' attention. From the model proposed by Puxley et al.[50], the mixed oxides exist in a uniform NiO-like phase in the calcined catalyst due to a strong interaction between the components oxides formed in the HTlc precursors. The introduction of copper does not change the structure, and the copper oxide would lose its structural features completely, even if the copper content is larger than aluminum [51].

2 Experimental Methods

The chapter includes information on the synthesis methods, characterization methods, and conversion tests. The synthesis methods that have been used in this project include the traditional constant pH titration method (including both high-saturation and low-saturation) and the new urea hydrolysis method (which uses urea to provide the anions needed to form HTlc particles). The characterization methods include Scanning Electron Microscopy (SEM), X-ray Diffraction (XRD), Transmission Electron Microscopy (TEM), Master-Sizer®, and Atomic Absorption Spectroscopy (AAS) which provides liquid phase analysis. Conversion tests were applied to the final catalyst using the coprecipitated HTlc particles as precursors.

2.1 Sample Preparation

2.1.1 Constant pH Titration

In a 600 mL beaker from Fisher 300 mL of de-ionized water was preheated to 80℃. Strong magnetic stirring was applied throughout the titration process. A mixture solution of sodium carbonate and sodium hydroxide with a concentration ratio 3:1 was co-added drop by drop with a mixture solution of the metal salts into deionized water. The nickel, aluminum and copper molar ratio was fixed 73:25:2. Deionized water was occasionally added into the bulk solution to compensate for evaporation and keep the total bulk volume at 300 mL. The bulk pH value was monitored by a Fisher® Accument AB15 pH meter, and was controlled around 10 (± 0.1) by adjusting the dropping speed of base solution and metal salts solution throughout the process.

The tips of the two titration burettes were kept close to each other to maximize the mixing efficiency. The equipment setup is shown in Figure 2.1.

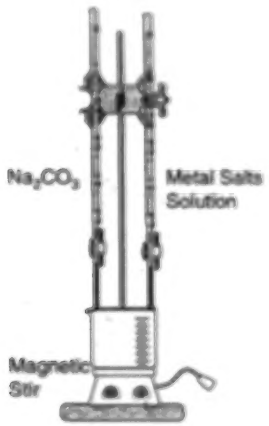

Figure 2.1 Titration equipment set.

The constant pH titration method was used to provide a comparison between the samples prepared in a constant pH environment and those prepared in an increasing pH environment.

2.1.2 Increasing pH Titration

The increasing pH titration process uses roughly the same equipment as the constant pH titration process, except the preheated liquid was 300 mL metal salts solution instead of pure de-ionized water. The mixture of base solution (sodium carbonate: sodium hydroxide = 3:1) was then added drop by drop into the bulk solution. The increasing pH value together with temperature were collected through a pH meter-computer interface unit and imported to a computer.

The primary use of the increasing pH titration method was to imitate the bulk coprecipitation method in which the hydrolysis of urea slowly liberates base ions resulting in an increasing bulk pH value. A comparison between the samples prepared by increasing pH titration and increasing pH bulk coprecipitation would be able to help identify how sodium affects the activity of the catalyst in the final product.

2.1.3 Increasing pH Bulk Coprecipitation Using Urea

Most of the nickel-aluminum based HTlc samples in this project were prepared by the method of bulk coprecipitation with increasing pH. Urea was used in this process to provide the anions needed to form HTlc crystals and eliminate the existence of sodium at the same time. Sodium has been proven to be detrimental to the catalyst activity [35]. The experimental equipment setup is shown in Figure 2.2.

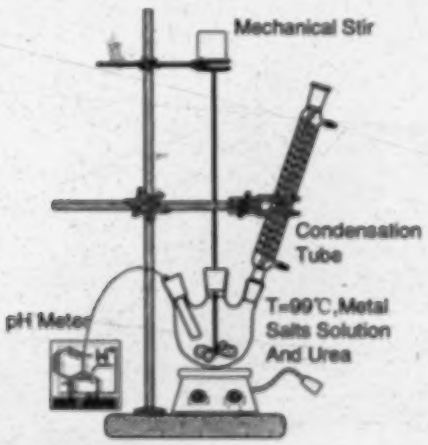

Figure 2.2 Coprecipitation equipment set.

Bulk coprecipitation was carried out by dissolution of nickel, aluminum and cupric nitrates in 300 mL of distilled water to a predetermined concentration varying from 0.05 mol/L to 1.2 mol/L, while the ratio among nickel, aluminum and copper

remained at 73:25:2. The solution was transferred to a 500 mL three-neck flask equipped with a condenser, a mechanical stirrer and a pH probe with thermometer. The solution was brought to 90℃ under strong mechanical stirring before solid urea was added into the flask. The size of the coprecipitated particles was monitored at different stages of the reaction before drying using a Malvern SM2000 Master-Sizer®. Samples for x-ray diffraction (XRD) and atomic absorption spectroscopy (AAS) tests were also picked at different stages of the process. All the samples were filtered, washed and centrifuged. The liquid parts of the samples were extracted for AAS tests, while the solid parts were further dried and ground for XRD tests.

Different urea concentrations and reaction temperatures were used in these experiments with PTR (PTR, the Practical-Theoretical Ratio, is the ratio between the amount of urea that was used in the experiment and the stoichiometric value. Refer to "Nomenclature") ranges from 1.0 to 9.0 and reaction temperature ranges from 60℃ to the highest temperature that could be reached (99.5℃). All chemicals used in these experiments, including metal nitrates and urea, were from Fisher Scientific and of Analytical Grade or better. Constant mechanical stirring was applied throughout the coprecipitation process. The electrode for the pH meter was approximately 2.5 centimeters below the water level inside the flask to ensure an accurate measurement. A PH meter-computer interface unit connector was used to collect and transfer pH data from the pH meter into a computer. The pH data were then reorganized and analyzed thoroughly.

2.2 Characterization Methods

The physical morphology and structure of coprecipitated HTlc particles and the nano-carbon fibers formed by decomposing methane, and the chemical composition of the bulk solution were investigated using different characterization methods.

Master-Sizer®

A Malvern SM2000 Master-Sizer® was used as the main equipment to measure the average size and the size distribution of the newly coprecipitated HTlc particles. The powder of the samples was dispersed using a small sample unit before measured by Malvern SM2000 Master-Sizer®. The average particle size and particle size distribution were measured by light scattering using a laser. The analysis of particle size was mainly based on data from the Master-Sizer instead of SEM or XRD.

X-ray Diffraction (XRD)

The coprecipitated nickel-aluminum based HTlc particles were dried in a vacuum oven overnight after washing and filtration. Structural analysis of the precipitates was carried out using a Rigaku Geigerflex 2173 Vertical Goniometer (X-ray tube: AEG FK 61-10 Co, X-Ray Source: Cobalt.) with $\lambda = 0.178897$ nm. The XRD pattern was then compared with the indexed XRD patterns of similar compounds. The main purpose of XRD scanning was to identify different phases of precipitates formed at different coprecipitation stages.

Solution Characterization: Atomic Absorption Spectroscopy (AAS)

The bulk solution after filtration and centrifuging was collected and characterized using AAS to determine the concentration of each metal cation, and hence their ratios. The samples were analyzed using a VARIAN 220FS Atomic Absorption Spectrophotometer. The ratio between nickel and copper and that between the divalent and trivalent metals in total were considered to be more important than the absolute value of the concentration of each metal cation because the ratios between different metal cations could be useful indicators of individual coprecipitation stages.

Scanning Electron Microscopy (SEM)

The coprecipitated nickel-aluminum based HTlc particles were scanned by a HITACHI S-2700 SEM (accelerating voltage = 20 kV) after washing and ultrasonication. The primary use of the SEM was to produce an overall image of particle morphology, but not to do any structural analysis.

Transmission Electron Microscopy (TEM)

A Philips EM 420 Transmission Electron Microscopy (TEM) was used at an accelerating voltage = 100 kV to obtain higher resolution images of the synthesized nano-carbon fibers. The size, structure and physical morphology of the carbon fibers was the main purpose of TEM scanning.

2.3 Conversion Test

The quality of the catalyst, especially the activity and durability of the prepared samples, was measured by the conversion rate of decomposing methane into hydrogen and carbon fibers in a furnace heated to 670℃. The effluent gas, which mainly consisted of methane, hydrogen and nitrogen (acted as dilution gas), was sent to a Micro-Gas Chromatography to measure the relative percentage in the mixture. The composition of the effluent gas was then compared with the feed gas, from which a conversion rate was calculated. The equipment for conversion tests is shown in Figure 2.3.

Figure 2.3 The equipment used to characterize the catalytic activity of the catalyst.

3 Results and Discussion

3.1 General Results

3.1.1 Coprecipitated HTlc Particles: Effects of Coprecipitation Parameters

Cavani et al. [1] carried out detailed structural investigations on HTlcs. It is now well established that HTlcs have a brucite-like structure with some Mg^{2+} ions being substituted by trivalent ions of similar atomic/ ionic radius. The net positive charge is compensated for by $CO3^{2-}$ ions. Both Adachi-Pagano [41] and Ogawa and Kaiho [57] presented SEM micrographs of the HTlc particles they synthesized. In their study, a clear octahedral lamellar structure was identified. Although XRD patterns proved the formation of pure HTlc particles, the HTlc particles synthesized in this project did not show the clear crystal structure as described by former researchers. The particles coprecipitated in this study were washed and then scanned by SEM. Figure 3.1 provides a close look at these micron-sized particles.

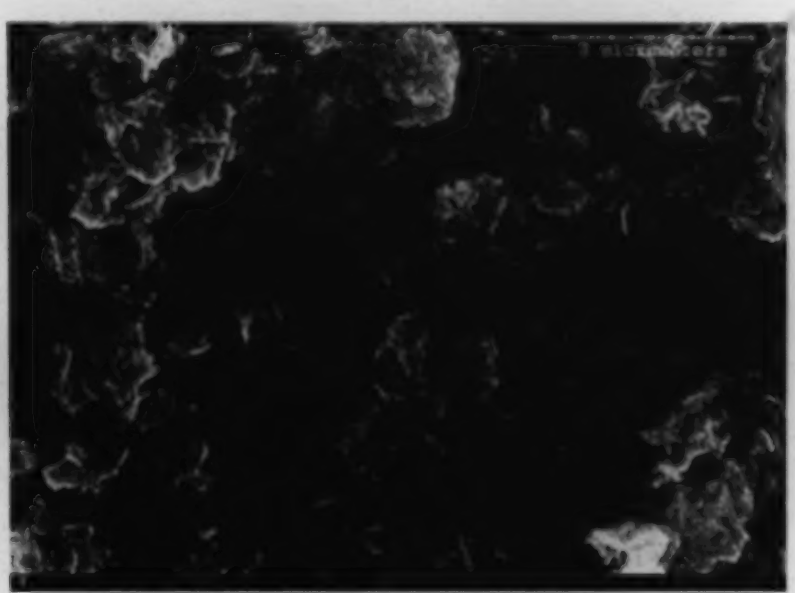

Figure 3.1 SEM micrograph of HTlc particles prepared by urea hydrolysis coprecipitation.

Aggregates formed by strong edge-surface platelet interactions are observed in the SEM micrographs of the prepared samples (Figure 3.1). This type of morphology was considered by Adachi-Pagano and his co-workers to be induced by the conditions of high base supersaturation which was imposed by the high pH coprecipitation conditions generally used in the constant pH method [41]. The broad particle size distribution caused by intensive agglomeration has greatly reduced the possible applications of the coprecipitated HTlc particles.

Use of the urea hydrolysis method should generate mono-dispersed HTlc particles, and a narrow particle size distribution could be obtained under high urea concentration and high reaction temperatures [41]. However, the so-called "sand rose" morphology was observed in this study, when relatively high urea concentration was applied, which was originally intended to produce smaller particles with a narrower particle size distribution. SEM and XRD analysis proved that smaller particles were generated under high PTR conditions. In contrast, the results from Master-Sizer® show that large particles were formed. At the same time, more "sand rose" morphology could be seen from the samples produced under high PTR conditions. This observation seems to indicate that the particles with "sand rose" morphology are the agglomerates of many separate hexagonal crystals. Agglomeration is anticipated to take place to a large extent when a large quantity of excess urea is present. The agglomeration can be seen from comparison between the SEM micrographs of the particles prepared in low (PTR = 3.0) and high (PTR = 9.0) relative urea concentration environment (Figures 3.2 and 3.3).

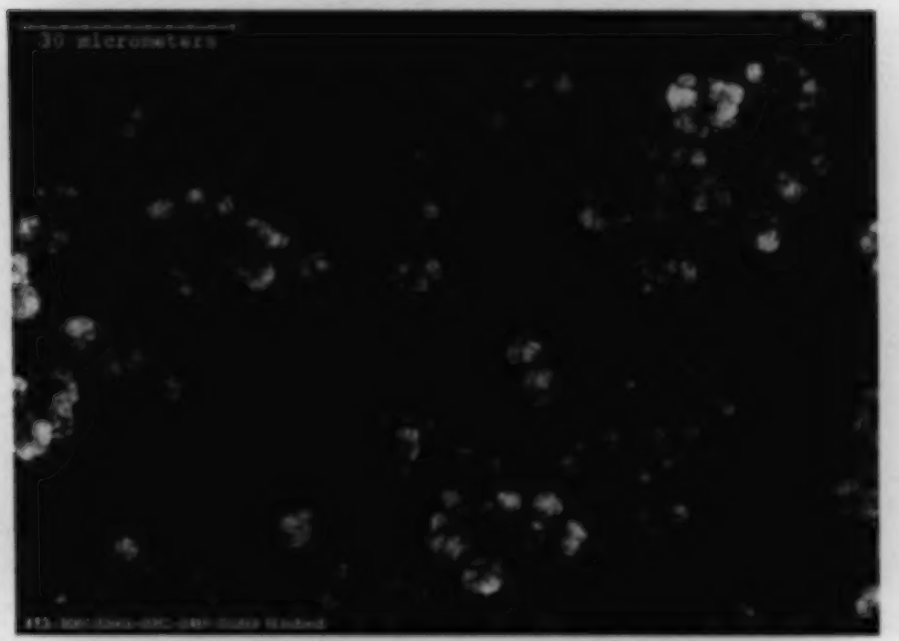

Figure 3.2 SEM micrograph of HTlc particles prepared by coprecipitation. PTR = 3.0, TMC = 0.4 mol/L, t = 24h, T = 99℃. Samples were washed thoroughly with water after filtration and centrifugation.

Figure 3.3 SEM micrograph: HTlc particles prepared by coprecipitation. PTR = 9.0, TMC = 0.4 mol/L, t = 24h, T = 99℃. Samples were washed thoroughly with water after filtration and centrifugation.

Although a smaller particle size was obtained by using high PTR, extensive agglomeration greatly increased the apparent particle size and caused the "sand rose" morphology. Since the "sand rose" morphology would lead to a very low specific surface area with nearly no porosity [41] and the aggregates are quite resistant to dispersion (remain aggregated and stable even under powerful ultrasonic treatments), it is necessary to eliminate the presence of the "sand rose" morphology. The extensive agglomeration together with the overlap of particle growth and nucleation caused a wider distribution of particle sizes. A delicate balance between particle size distribution and particle morphology could be reached under certain reaction temperatures and urea concentration. Detailed discussion will be given in a later section.

3.1.2 Coprecipitation Reaction Scheme

Several hypothetical reaction schemes of the coprecipitation process using urea hydrolysis were proposed by earlier researchers. Boclair and Braterman [40] proposed the formation of solid $M(III)(OH)_3$ as an intermediate product before HTlc particles are precipitated. Meanwhile, Rao et al. [42] proposed another hypothetical reaction scheme which includes the formation of several intermediates such as $Mg(OH)(H_2O)^{+}_{n}$ and $Al(OH)(H_2O)^{2+}_{m}$. Adachi-Pagano et al. [41] also proposed the formation of an "aluminum aquo hydroxo complex" and the possible precipitation of solid $Al(OH)_3$ in an Al-Mg system.

In this study, several comparison tests are carried out to look into the reaction scheme. The effects of several reaction parameters such as PTR, reaction temperature and reaction time are investigated and discussed. From these controlled tests, the precipitation sequence, possible intermediate products, and an alternative reaction scheme are proposed in a later section.

3.2 Effect of Coprecipitation Parameters On Particle Size And Morphology

3.2.1 Effect of PTR

PTR, the Practical-Theoretical Ratio for urea, presents the mole ratio between the amount of urea that was used in the experiment and the stoichiometry amount, i.e., theoretical amount of urea needed to precipitate all the metal cations present in solution. For example, if the concentration of the cations (Ni: Al: Cu = 73:25:2) is 0.12 mol, a theoretical amount of 0.12 mol urea is required to precipitate all the metal cations in solution, then a PTR = 3.0 indicates that we use 0.36 mol urea to precipitate the metal cations in this specific experiment.

The effect of PTR on the rate of pH evolution rate can be clearly seen in Figure 3.4, in which the bulk pH values measured at different reaction time were plotted as a function of reaction time. The curve was defined as "bulk pH curve" in this article.

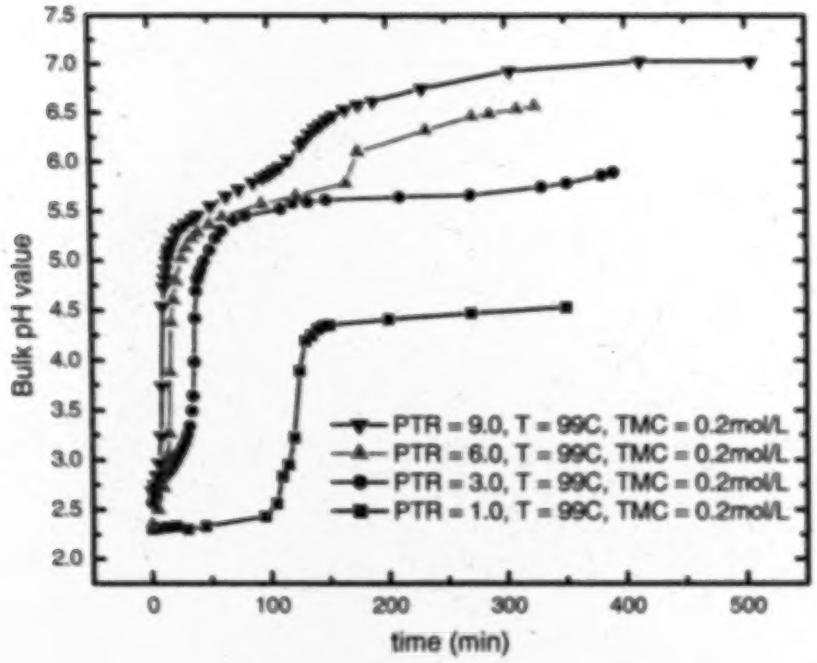

Figure 3.4 Bulk pH curves under different PTR values.

A higher PTR causes an increase in pH at inflection point over a shorter period, indicating a higher reaction rate. It can be seen from Figures 3.5 and 3.6 that the reaction rate increased by a factor of 50 when PTR increased from 1.0 to 9.0. These results indicate that the reaction rate is very sensitive to PTR.

Figure 3.5 sheds more light on the effect of PTR on reaction rate. A positive linear relationship was shown between the PTR and reciprocal of reaction time to reach a bulk pH of 4.5. The pH value of 4.5 is selected because the first stage of coprecipitation, or the first buffer region of the bulk pH curve, usually ends around this pH value. A higher PTR accelerates the reaction rate, thus less time is needed to reach a certain bulk pH value. A similar relationship can be observed in Figure 3.6 when bulk pH = 6.5 was set as another milestone.

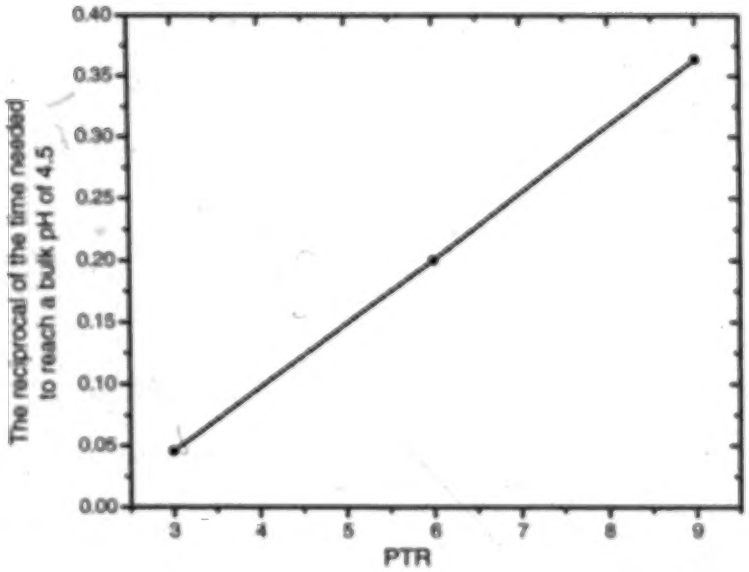

Figure 3.5 The reciprocal of the time needed to reach a bulk pH of 4.5 at different PTR values.

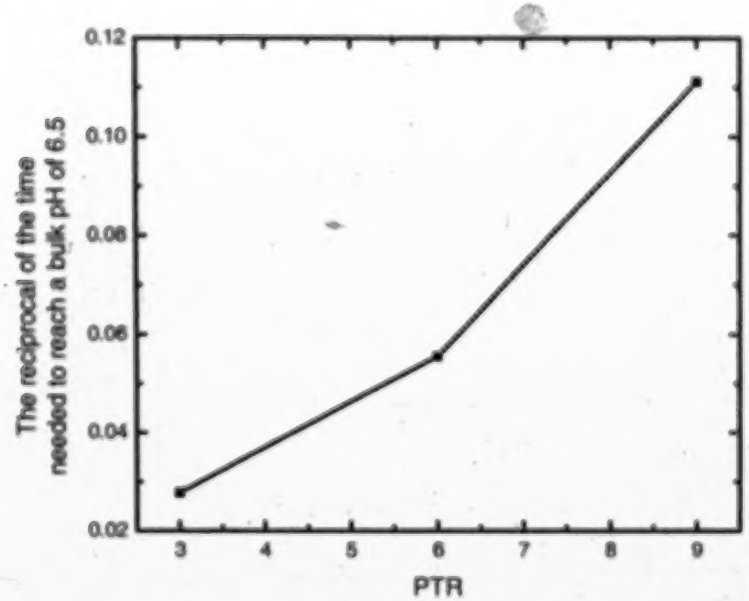

Figure 3.6 The reciprocal of the time needed to reach a bulk pH of 6.5 at different PTR values.

The effect of PTR on coprecipitation is not limited to reaction rate. The average particle size and particle size distribution also show a clear correlation to PTR. In general, a system with a higher PTR value, which indicates a higher relative urea concentration, provides more anions (OH^- and CO_3^{2-}) to help the nucleation of the HTlc precipitation. Consequently, smaller particles could be obtained under these conditions. The results of this study showed some discrepancies with this conjecture. A decrease in the average particle size was observed when PTR increased from 1.0 to 4.0 as anticipated. However a sharp increase in the average particle size was observed when PTR continued to increase to 9.0. Figures 3.7 and 3.8 showed the effects of PTR value on average particle size for reaction times of 6 and 24 hours, respectively.

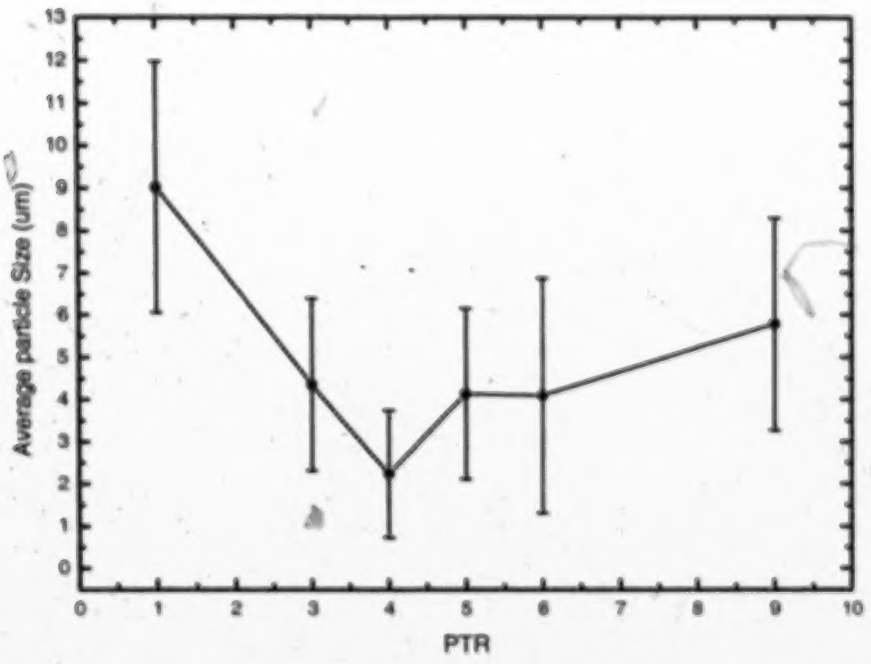

Figure 3.7 Average particle size as a function of PTR, with t = 6 h, TMC = 0.4 mol/L, reaction temperature = 99 ℃.

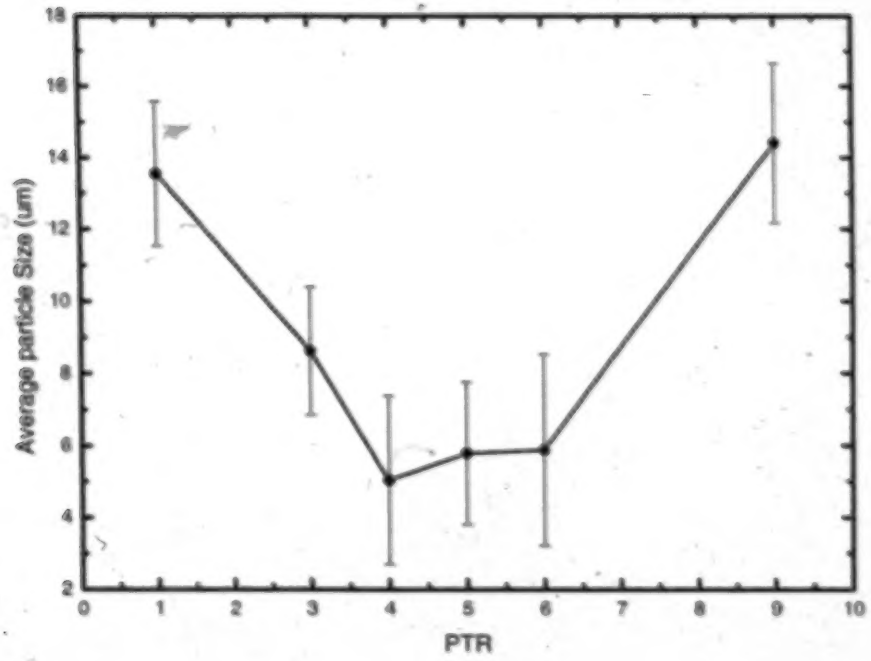

Figure 3.8 Average particle size as a function of PTR, with t = 24 h, TMC = 0.4 mol/L, reaction temperature = 99 ℃.

Both figures show a decrease in average particle size can be observed when PTR increased from 1.0 to 4.0. According to Shaw and Bordeaux [38], hydrolysis of urea proceeds in two steps, the formation of ammonium cyanate (NH_4CNO) as the rate determining step, and the fast hydrolysis of the cyanate to ammonium carbonate.

$$NH_2\text{–}C\text{=}O\text{–}NH_2 + 2H_2O \longrightarrow 2NH_4^+ + CO_3^{2-} \quad \text{(Overall)} \qquad (3.1)$$

$$NH_2\text{–}C\text{=}O\text{–}NH_2 \longrightarrow NH_4^+ + NCO^- \qquad (3.2)$$

$$NCO^- + 2H_2O \longrightarrow NH_4^+ + CO_3^{2-} \qquad (3.3)$$

Although the hydrolysis of urea can be greatly accelerated by increasing reaction temperature, the rate of anions released (OH^- and CO_3^{2-}) is still relatively slow compared to the large amount required by the metal cations. As a direct consequence of the low concentration of anions, a large part of the anions released by urea is consumed by particle growth, and little for nucleation. Agglomeration is also limited due to low concentration of primary particles. Therefore, under low PTR values, the particle growth is the predominant reaction and the size of precipitates increases with the amount of available anions (OH^- and CO_3^{2-}).

When PTR was increased from 6.0 to 9.0, a sharp increase in secondary particle size was observed. This increase in secondary particle size was attributed to the extensive agglomeration that took place when excess anions (OH^- and CO_3^{2-}) were present in solutions of high relative urea concentrations. More detailed information could be obtained from the SEM micrographs of samples produced under different PTR.

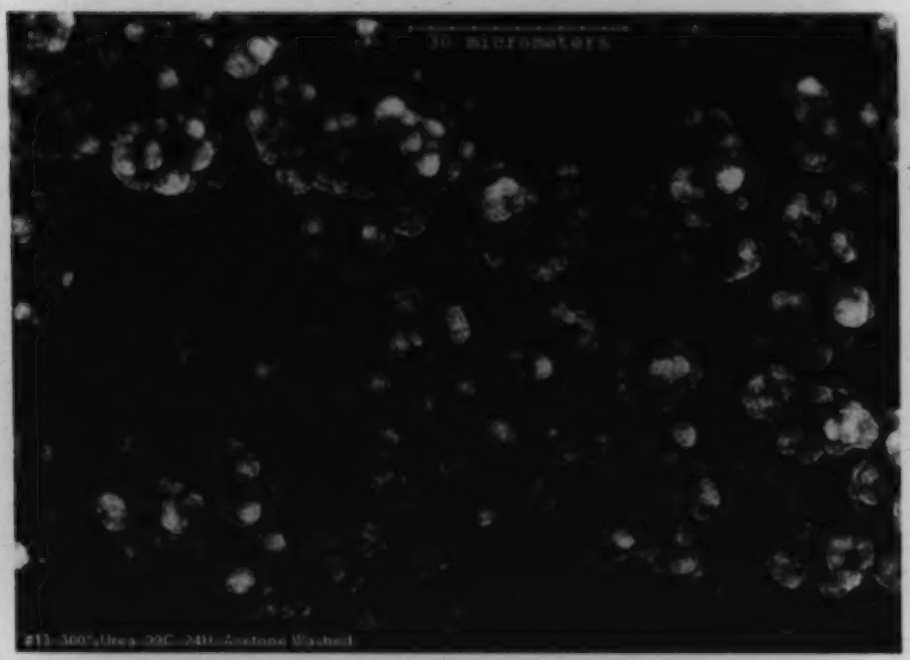

Figure 3.9 SEM micrograph of HTlc particles precipitated by urea hydrolysis. PTR = 3.0, TMC = 0.4 mol/L, t = 24 h, T = 99 ℃. Samples were washed thoroughly with water and acetone after filtration and centrifugation.

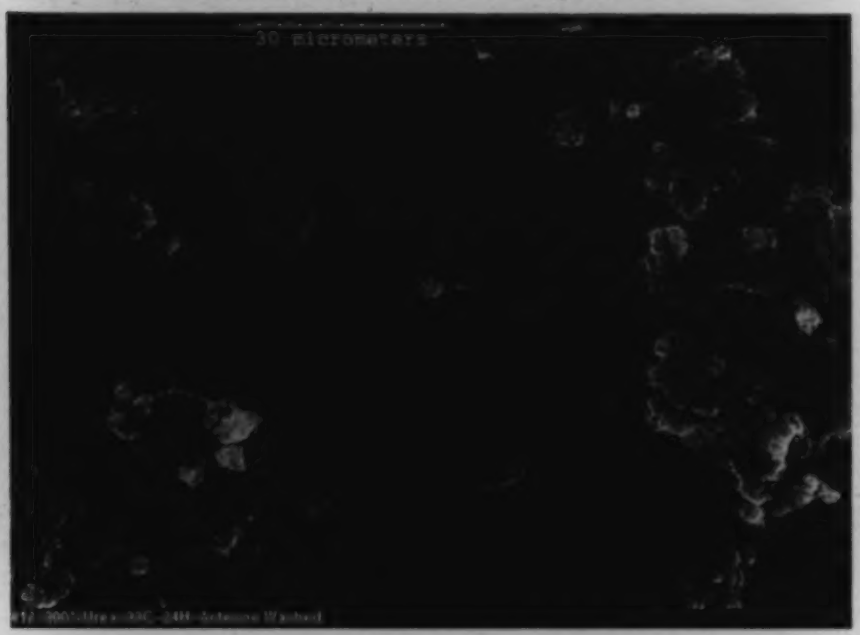

Figure 3.10 SEM micrograph of HTlc particles precipitated by urea hydrolysis. PTR = 9.0, TMC = 0.4 mol/L, t = 24 h, T = 99 ℃. Samples were washed thoroughly with water and acetone after filtration and centrifugation.

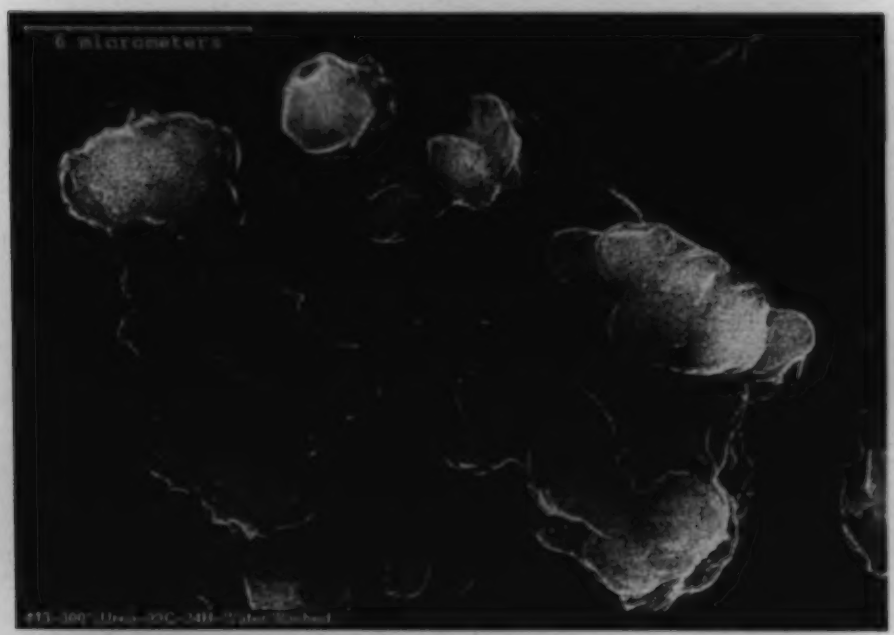

Figure 3.11 SEM micrograph of HTlc particles prepared by coprecipitation. A closer view of the particles synthesized at PTR = 3.0, TMC = 0.4 mol/L, t = 24 h, T = 99 ℃. Samples were washed thoroughly with water after filtration and centrifugation.

Figure 3.12 SEM micrograph of HTlc particles prepared by coprecipitation. A closer view of the particles synthesized at PTR = 9.0, TMC = 0.4 mol/L, t = 24 h, T = 99 ℃. Samples were washed thoroughly with water after filtration and centrifugation.

A comparison of the SEM micrographs of the samples prepared under low urea concentration (PTR = 3.0) and high urea concentration (PTR = 9.0) shows the effect of urea concentration on both the primary particle size and secondary particle size (particles after agglomeration) (refer to Figures 3.9 - 3.12). The samples prepared under low urea concentration have noticeably larger primary particles compared to those precipitated under high urea concentration. However, the extensive agglomeration happened in the presence of a large amount of excess anions (OH^- and CO_3^{2-}), indicated by the appearance of the "sand rose" morphology. Such agglomeration made the secondary particles formed under high urea concentration even larger than those produced in low urea concentration environment.

The "sand rose" morphology was observed when coprecipitation was performed at constant pH and high degree of anion supersaturation [1]. Such a morphology led to low specific surface areas and almost zero porosity. The aggregates, once formed, were stable and resistant to re-dispersion even by powerful ultrasonic treatments [41, 39]. The potential applications of the precipitated particles were limited due to these negative attributes of "sand rose" morphology. The method of precipitation using temperature controlled urea hydrolysis has been suggested by Adachi-Pagano et al. [41] to be an effective method to avoid the formation of "sand rose" morphology while generating mono-dispersed particles. However, it would be wise to keep the relative urea concentration under a certain value to achieve this goal.

A calculation from XRD patterns of the same samples prepared under different PTR further confirmed the increase in primary particle size when PTR is reduced from 9.0 to 1.0. The primary particle size was calculated from the Scherer formula: D(hkl) =

$K\lambda / (\beta \cos(\theta_{hkl}))$, where $\lambda = \lambda(CuK\alpha) = 0.178897$ nm, β = peak width at half height (rad.), θ_{hkl} = Bragg angle, K = instrumental factor. The XRD patterns of samples are shown in Figures 3.13 and 3.14.

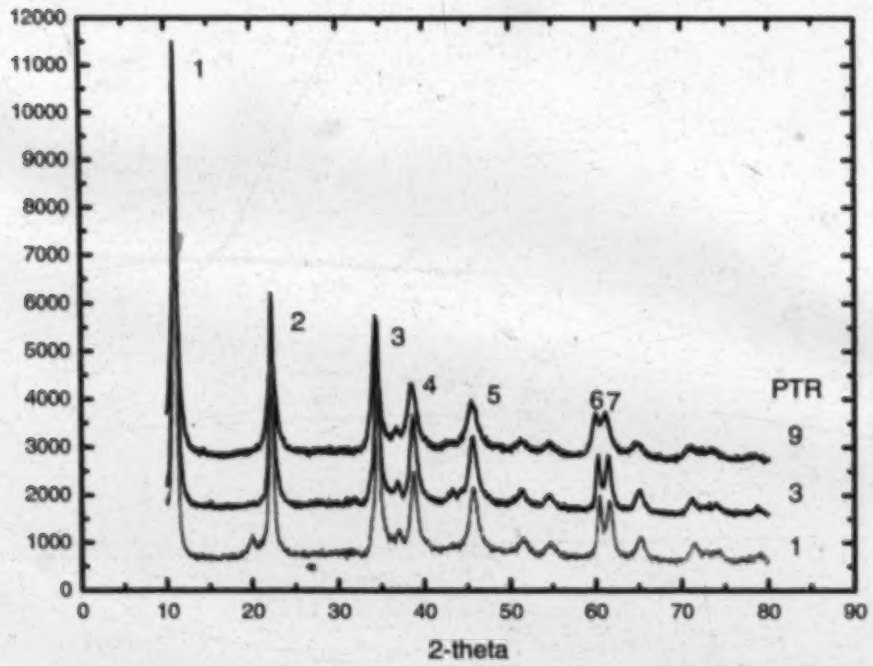

Figure 3.13 XRD patterns of samples prepared under different PTR, with t = 24h, T = 99℃ and TMC = 0.2 mol/L.

	FWHM					
	Reaction time t = 24h			Reaction time t = 6h		
Peak Number	PTR=9	PTR=3	PTR=1	PTR=9	PTR=6	PTR=3
1	0.96	0.55	0.52	0.95	0.75	0.54
2	1.01	0.57	0.55	1.00	0.75	0.55
3	0.76	0.55	0.51	0.75	0.77	0.53
4	1.25	0.85	0.90	1.25	0.99	0.91
5	1.37	1.12	1.05	1.34	1.14	1.06
6	1.98	0.71	0.73	1.99	0.93	0.73
7	1.09	0.57	0.75	1.10	0.75	0.55

Table 3.1 FWHM of peaks of Figures 3.13 and 3.14.

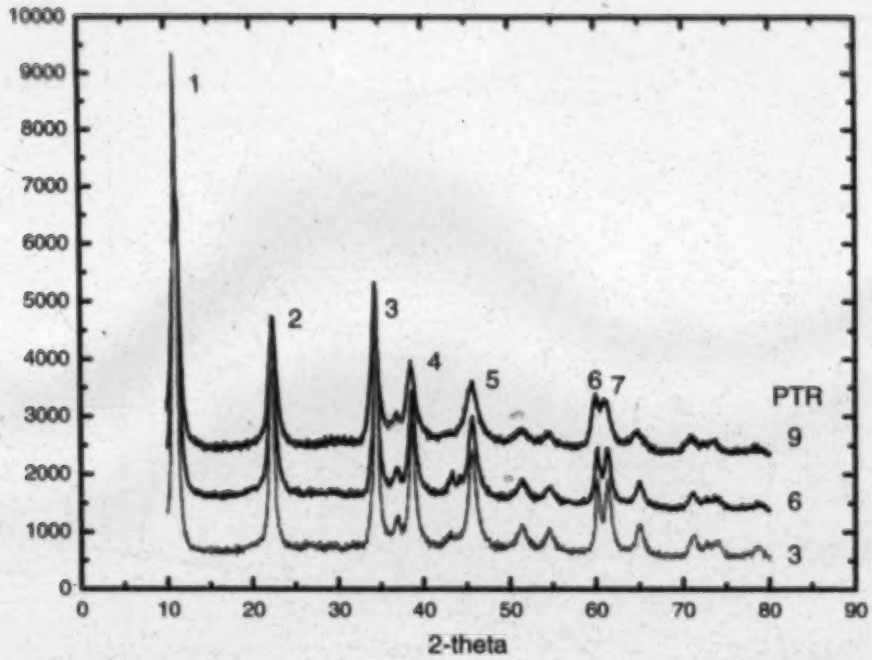

Figure 3.14 XRD patterns of samples prepared under different PTR, with t = 6h, T = 99℃ and TMC = 0.2 mol/L.

3.2.2 Effect of Reaction Time

The coprecipitated particles tend to grow and agglomerate as aging time is extended. In these experiments, samples were picked at different times of a coprecipitation process, with PTR = 3.0, TMC = 0.4 mol/L and T = 99℃. The samples were immediately diluted and cooled down to avoid further precipitation, precipitate growth and agglomeration. The particle size distribution of the sample was measured shortly after by Master-Sizer® 2000 immediately. The results are shown in Figure 3.15.

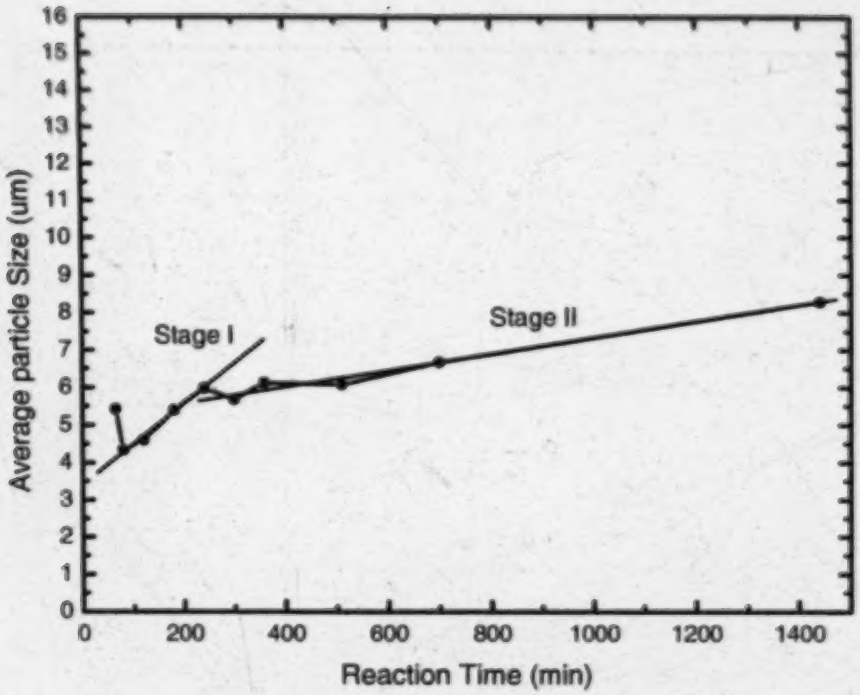

Figure 3.15 Average particle size of precipitates sampled at different reaction time, with T = 99℃, TMC = 0.2 mol/L and PTR = 3.0.

It could be inferred from the curve that both agglomeration and particle growth happened during the first 250 minutes (stage I), which is indicated by a sharper increase in the average particle size. However, the rate at which the particle size increased decreased when the reaction stepped into stage II, especially after approximately 400 minutes. The time where the turning occurs would probably change with changing urea concentration and reaction temperature. Both of these factors have a great effect on the reaction rate.

Figure 3.16 shows the average particle size of the precipitates synthesized under different reaction conditions. An increase in average particle size could be observed

when reaction time was extended from 6h to 24 h under all PTR values. Adachi-Pagano et al. [41] reported that once the pH reached its plateau value (the "plateau", in this article, is defined as the buffer region occurred in the bulk pH curves, as shown in Figure 3.4) after about 3 hours, the particle growth became the determinant reaction. However, the sharp increase in particle size when PTR = 9.0 goes beyond the expectation of particle growth.

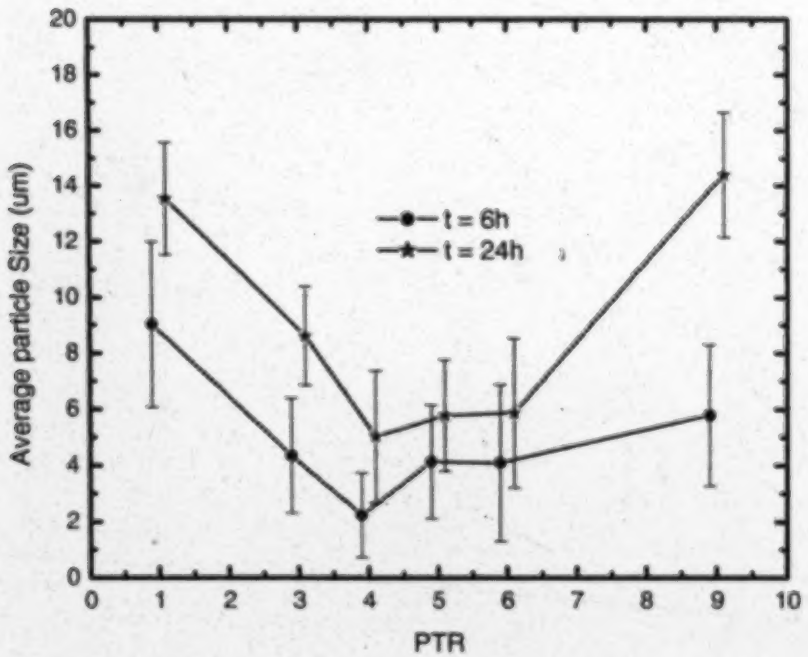

Figure 3.16 Average particle size of precipitates synthesized under different PTR with T = 99℃ and TMC = 0.2 mol/L. Also a comparison between the samples picked at t = 6h and t = 24h.

Agglomeration was suspected to be one of the main reasons to account for more than double of particle size over the last 18 hours. Several SEM micrographs of the samples (Figures 3.17a – d) picked at different reaction times provide further information on this point.

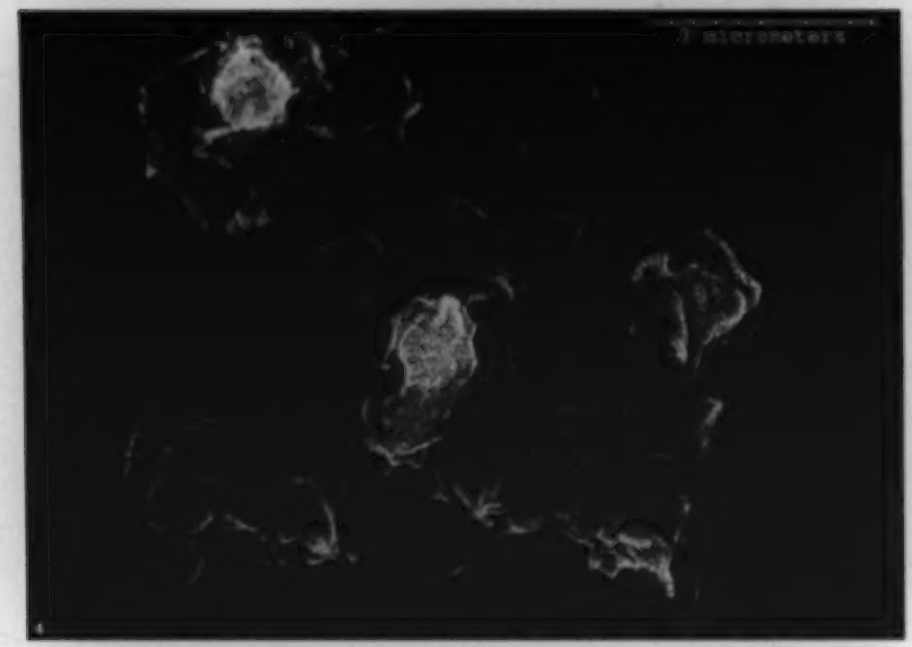

Figure 3.17.a SEM micrograph of particles precipitated at t = 2 h. PTR = 9.0, T = 99 ℃, TMC = 0.4 mol/L.

Figure 3.17.b SEM micrograph of particles precipitated at t = 5 h. PTR = 9.0, T = 99 ℃, TMC = 0.4 mol/L.

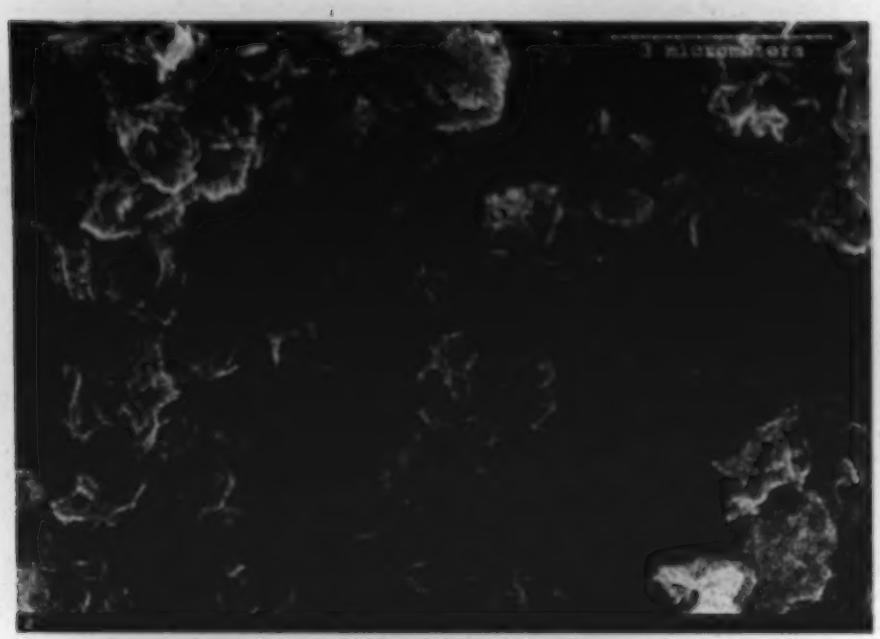

Figure 3.17.c SEM micrograph of particles precipitated at t = 10 h. PTR = 9.0, T = 99 ℃, TMC = 0.4 mol/L.

Figure 3.17.d SEM micrograph of particles precipitated at t = 24 h. PTR = 9.0, T = 99 ℃, TMC = 0.4 mol/L.

The growth of the "sand rose" morphology indicates that agglomeration was aggravated as reaction time was extended. It can be thus concluded that when PTR is low, i.e., in a low relative urea concentration environment, particle growth is the dominant reaction after initial coprecipitation depending on reaction temperature and urea concentration. This is the main reason for the increase in average particle size measured by Master-Sizer®. However, when PTR is high, i.e., in a high relative urea concentration environment, agglomeration took place extensively even after several hours of reaction, which brought a faster increase in average particle size.

Although becoming more and more agglomerated, the crystalline structure of the precipitates does not change with reaction time. A comparison between the XRD patterns from the 6h sample and the 24h sample (Figures 3.18 and 3.19) supports this conjecture.

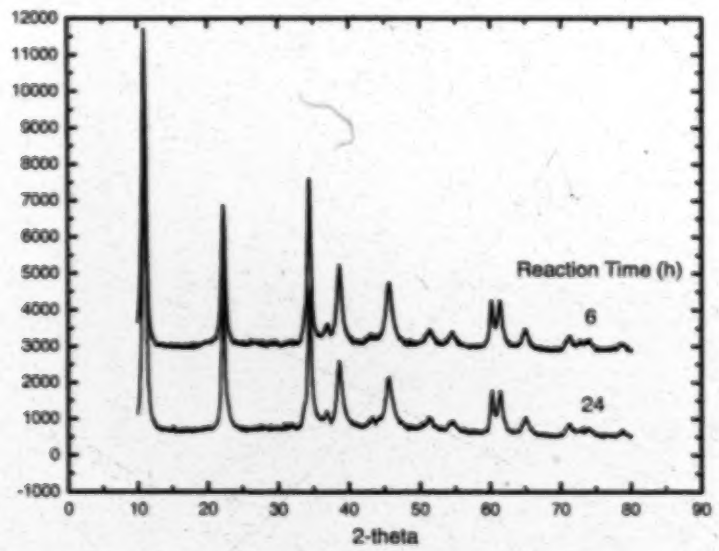

Figure 3.18 XRD patterns of samples picked at t = 6 h and t = 24 h, under reaction conditions of PTR = 3.0, TMC = 0.2 mol/L, T = 99 ℃.

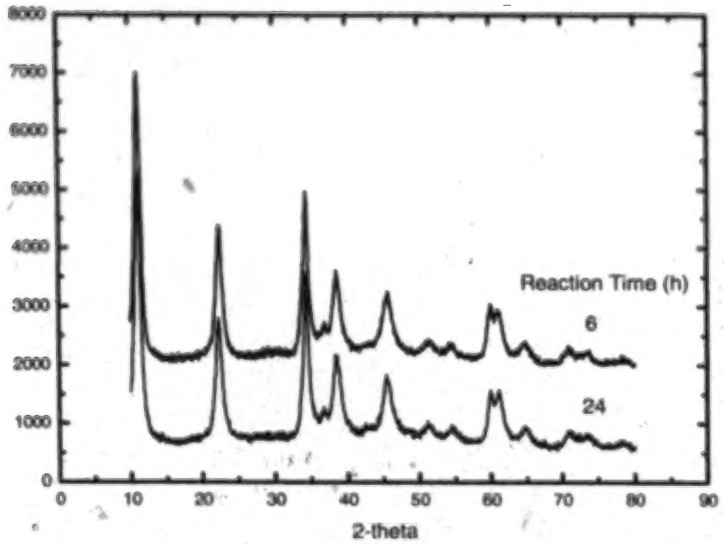

Figure 3.19 XRD patterns of samples picked at t = 6 h and t = 24 h, under reaction conditions of PTR = 9.0, TMC = 0.2 mol/L, T = 99 ℃.

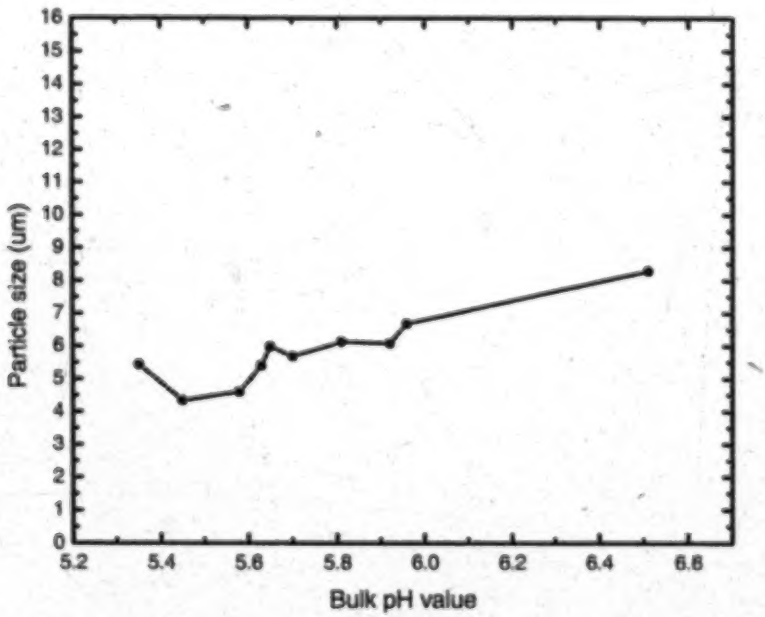

Figure 3.20 Average particle size (um) as a function of bulk pH value. All the pH values are measured at 99 ℃.

As the pH value of bulk solution increases with time, the particle size also shows some relationship with the bulk pH value (Figure 3.20). In fact, the composition of the coprecipitated particles, including the ratio between divalent and trivalent metals and the ratio between different divalent metals also changes slightly with pH value of bulk solutions and reaction time. More detailed discussion on the relationship between precipitate composition and the reaction time/ bulk pH value will be given in section 3.3.

3.2.3 Effect of Reaction Temperature

The effect of reaction temperature on the average size and particle size distribution of the synthesized HTlc particles is manifested through its effect on the urea decomposition rate. Urea decomposition provides hydroxides and carbonates for HTlc precipitation reaction. The urea decomposition rate depends greatly on the reaction temperature. Other researchers reported an increase in reaction rate constant by about 200 times when the reaction temperature was increased from 60℃ to 100℃ [41].

A large average particle size was obtained in this series of experiments when a lower reaction temperature (90℃) and lower PTR (PTR = 1.0) were used. At the low reaction temperature together with the low urea concentration, the release of hydroxides and carbonates is extremely slow, which in turn slows down the particle precipitation rate and favors particle growth, as discussed above. A larger average particle size with a broader particle size distribution was obtained when high reaction temperature (99℃) and high PTR (PTR = 9.0) were used. In this case, extensive

agglomeration contributed mainly to the increase in average particle size. The overlap of particle growth and generation led to products of broad particle size distribution.

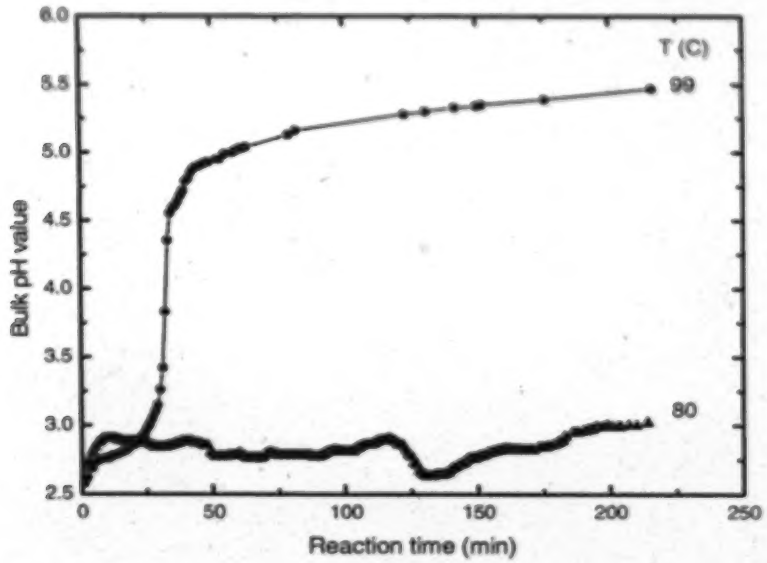

Figure 3.21 Bulk pH curves under different reaction temperatures. TMC = 0.2 mol/L, PTR = 4.0.

In addition to the effect on particle size, the reaction temperature also affects the reaction rate. In low PTR solutions, the bulk pH ceased to increase when reaction temperature was controlled around 80℃, as shown in Figure 3.21. At 99℃, a rapid increase in pH was observed at reaction time around 25 minutes. The transition temperature from slow to rapid reaction rate depends on PTR. In general, the transition temperature decreases with increasing PTR. For example, at PTR at 9.0, the transition temperature decreased to 70℃. Since the transition temperature is closely correlated with the relative urea concentration, it can be deduced that the effect of reaction temperature on the reaction rate is also mainly achieved through its effect on the rate of urea hydrolysis.

3.3 Coprecipitation Chemistry

3.3.1 Different Stages of Coprecipitation Process

Figure 3.22 shows the bulk pH curve obtained using urea under PTR = 1.0, T = 99 ℃ and TMC = 0.2 mol/L. Two distinct buffer regions, connected by a sharp rise in the transition period, are evident in the bulk pH curve of coprecipitation process.

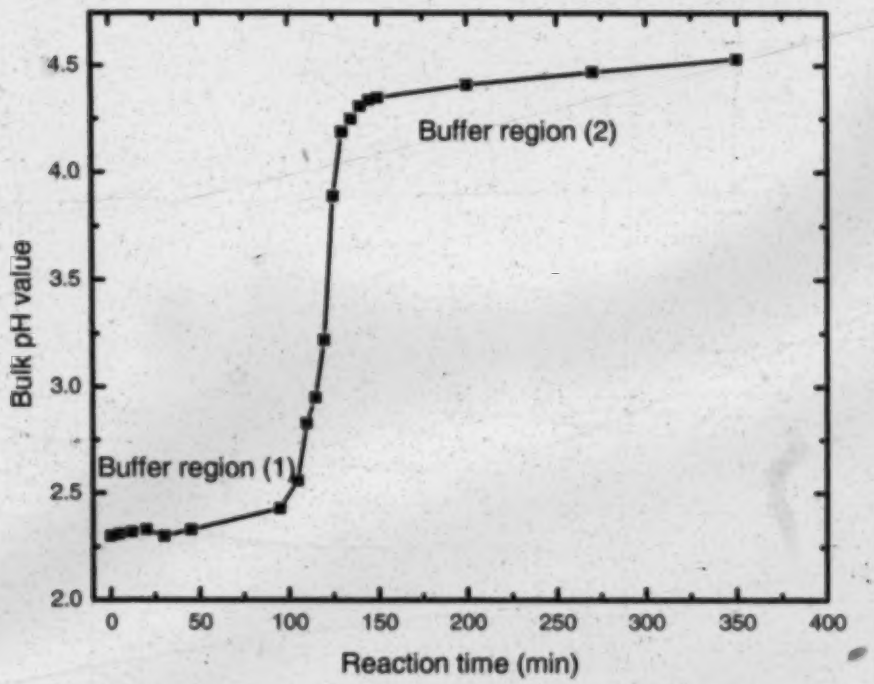

Figure 3.22 Bulk pH curve with clear two buffer regions. Ni-Cu-Al coprecipitation, PTR = 1.0, T = 99 ℃, TMC = 0.2 mol/L.

The buffer region (1), or the first plateau, can be very short depending on the reaction rate, which to a large extent is controlled by the reaction temperature and PTR. Compared to the equilibration rate in the buffer region (2), equilibrium in this region

is quite rapid, usually reached in a few seconds. Buffer region (2), or the second plateau, takes approximately 10 minutes to reach a constant pH value. Normally, the length of the first plateau diminishes with increasing reaction rate (Figure 3.23). However, the "height" of the first plateau, i.e., the starting pH and ending pH value, depends on only the activity and identity of the trivalent metals involved in the coprecipitation process. The "height" of the first plateau in the presence of multiple trivalent metal cations was not studied here. The transition portion from first to second plateau is usually sharp, which occurs in a few seconds. This is because the intermediate product of the trivalent metals can no longer absorb the hydroxyl ions released by the hydrolysis of urea.

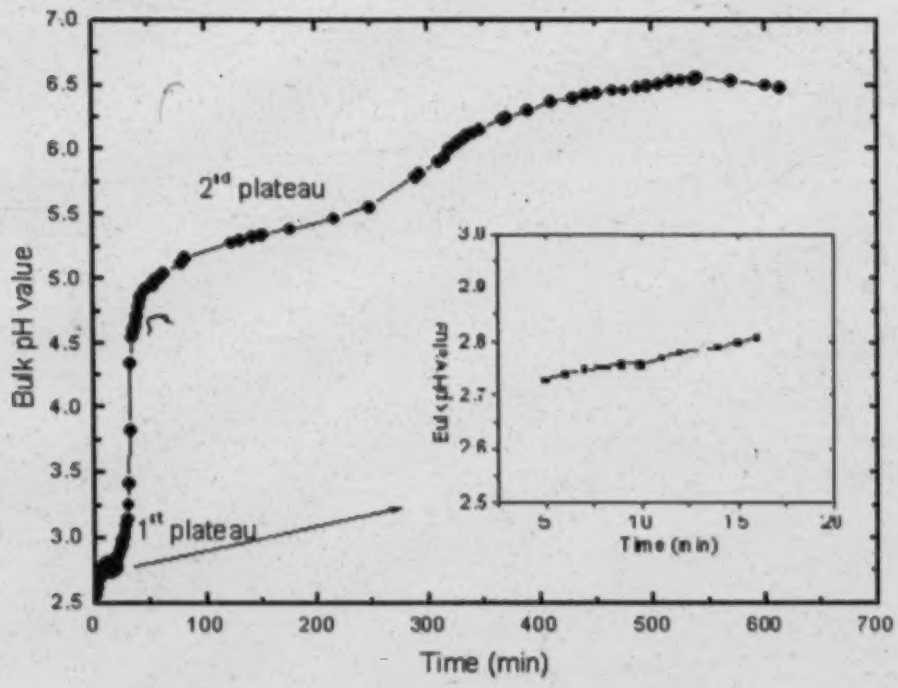

Figure 3.23 Accelerated reaction with PTR = 4.0, TMC = 0.2 mol/L and T = 99 ℃.

Understanding the two clear buffer regions is of great scientific and practical importance. In our experiments, a group of comparison tests was carried out to establish the relationship between the identity of the trivalent metal and the position of the first plateau. Figure 3.24 gives the bulk pH curve of two tests, both of which were carried out under the reaction temperature of 99 ℃, TMC = 0.2 mol/L and PTR = 4.0. The metal cation species and concentrations are as follows:

Test 1: 0.05 mol/L Al^{3+}, 0.15 mol/L Ni^{2+}

Test 2: 0.05 mol/L Fe^{3+}, 0.15 mol/L Ni^{2+}

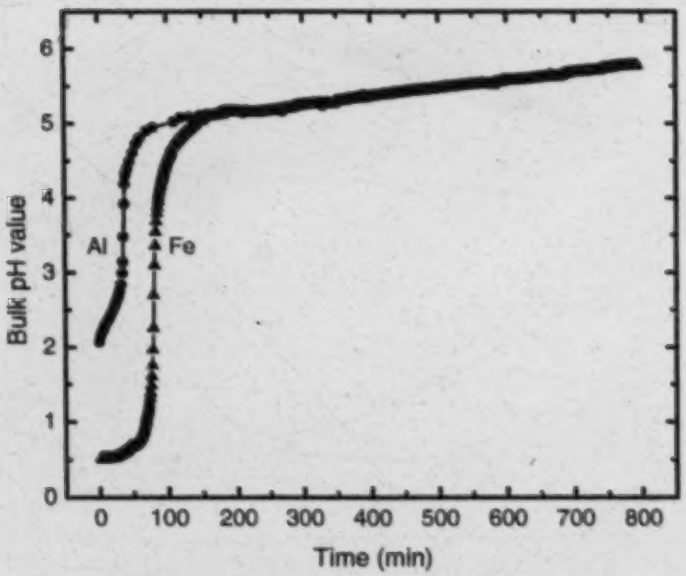

Figure 3.24 Bulk pH curves of comparison tests between Al-Ni system (25% Al + 75% Ni) and Fe-Ni system (25% Fe + 75% Ni) with PTR = 4.0, TMC = 0.2 mol/L and T = 99 ℃.

The two pH curves in Figure 3.24 share an almost identical "second plateau", while a large difference exists in the starting "points", which are actually shortened "first

plateau" due to the fast reaction rate. Since all other reaction parameters including bivalent metal ion concentration are identical in these two tests, the difference in the position of "first plateau" could only be explained by the difference of trivalent metal ions.

Similarly, the identity and character of the bivalent metal ions are the determinants of the "second plateau". Figure 3.25, as a counterpart of Figure 3.24, shows the pH curves of another group of comparison tests, which aims at ascertaining the effect of the bivalent metal ions on the position of the "second plateau".

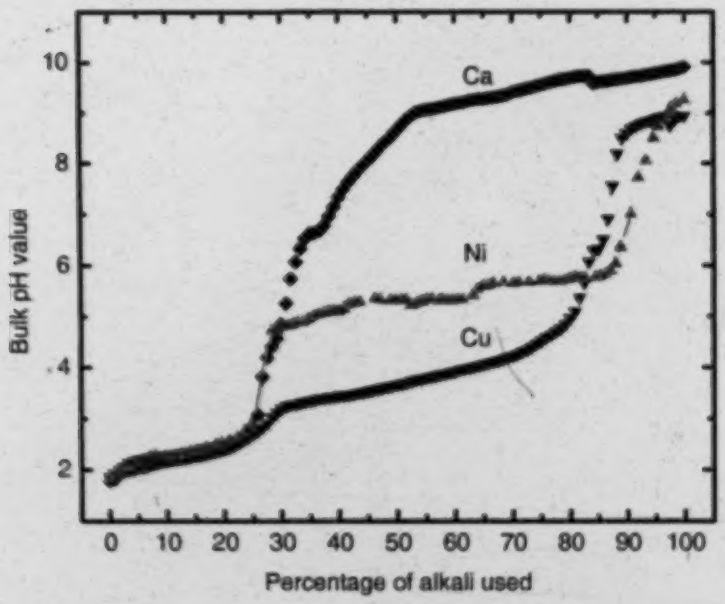

Figure 3.25 Bulk pH curves of comparison tests among Al-Ca, Al-Ni and Al-Cu systems. Titration of 3:1 $[M^{2+}]/[M^{3+}]$ solutions with TMC = 0.2 mol/L and T = 85 ℃.

The three pH curves show an identical "first plateau", which can be attributed to the common trivalent metal. The position (the bulk pH value) of the second plateau varies depending on types of divalent metal ions used in the tests.

3.3.2 Precipitation Sequence

In addition to the existence of multiple coprecipitation buffer regions, another point that deserves more attention is the precipitation sequence among different metal cations. It was apparent from this work that copper starts to precipitate at a relatively lower pH value compared with nickel, and thus starts to precipitate earlier than nickel during the coprecipitation process. A group of titration tests was designed to examine the precipitation pH value for different metal cations. The same sequence was confirmed by these tests, in which sodium carbonate were added into pure Cu, Ni and Al nitrate solutions. The pH curves for these titration tests are shown in Figure 3.26.

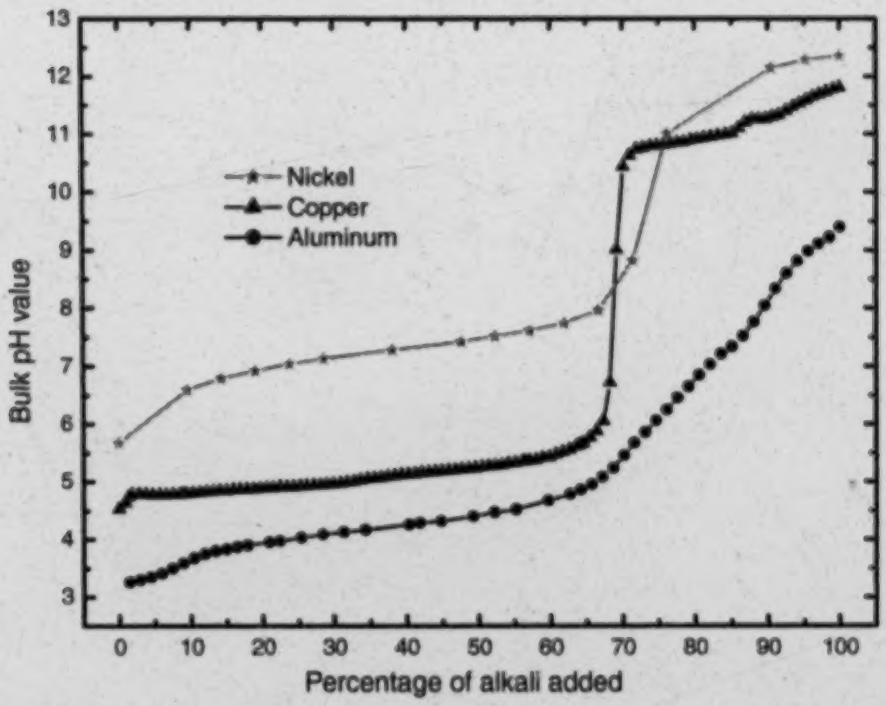

Figure 3.26 Bulk pH curves of titration test by Na_2CO_3 addition at room temperature and under vigorous stirring.

When multiple divalent metal cations are present in the solution, multiple-step sequential precipitation would occur with increasing bulk pH value. In the Ni-Cu-Al systems studied here, aluminum would be the first one to react with hydroxides released by urea hydrolysis, followed by copper, and then nickel. Figure 3.27 shows the atomic absorption spectroscopy (AAS) results that confirmed the sequence between the two divalent metal ions. The samples examined by AAS were the liquid part of the samples picked at different stages of the reaction. The sample slurries were diluted and cooled by adding de-ionized water immediately followed by centrifugation. The liquid part was extracted and prepared for AAS analysis.

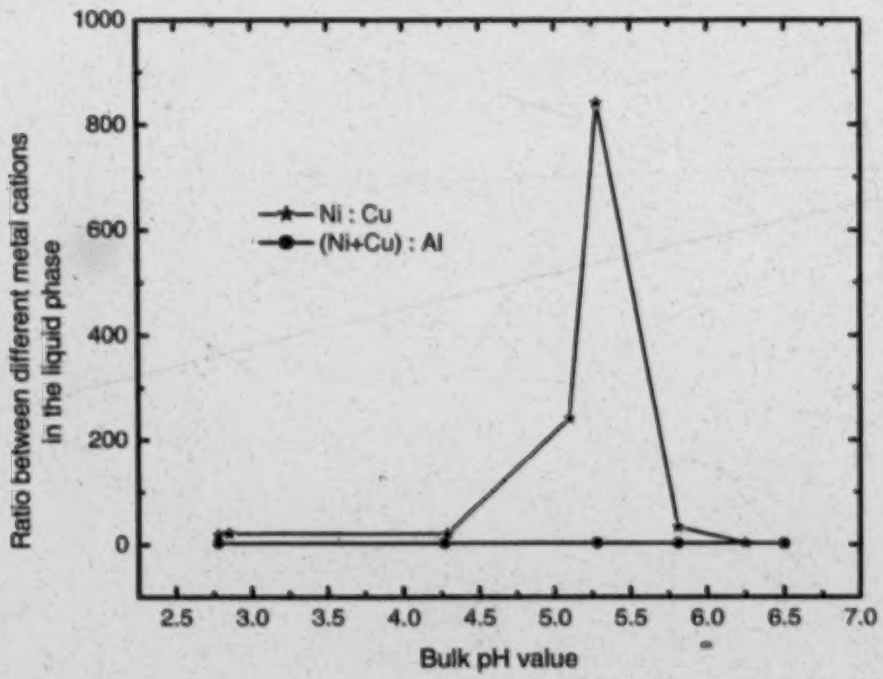

Figure 3.27 AAS results to investigate the precipitation sequence. The mole ratios of Ni: Cu and divalent metal: trivalent metal were examined in a Ni-Cu-Al system. Coprecipitation was performed at T = 99 ℃, PTR = 4.0 and TMC = 0.2 mol/L.

As the AAS samples are the residual liquid part of the samples taken at different stages of reaction, the sharp rise in the Ni: Cu ratio when the bulk pH value reaches 4.5 shows that copper precipitates much faster than nickel at this stage of reaction. As more and more nickel precipitates in later reaction stages, the Ni: Cu ratio returns to its original value at bulk pH above 6.5, which indicates full precipitation of both divalent metal cations.

Compared with Figure 3.23, in which the bulk pH curve for the same test is presented, it could be easily observed that the sharp rise in Ni: Cu ratio observed from the AAS solution analysis happened simultaneously with the sharp rise in the bulk pH value. When the bulk pH reaches its transition part (around pH = 4.5) from the first plateau to the second plateau, the Ni: Cu ratio starts to increase. When the bulk pH reaches its second plateau, the Ni: Cu ratio also increases rapidly and reaches its maximum value soon afterward. This correspondence indicates that the divalent metal ions would react with the hydroxide and carbonate liberated by urea, sequentially in the second or even the third plateau. Another interesting part of Figure 3.27 is the nearly constant ratio between divalent metal and trivalent metal throughout the reaction. This is the consequence of HTlcs formation, which requires a trivalent: divalent metal ratio ranging between 0.25 and 0.33.

However, strict sequential-precipitation does not usually occur. A slow decrease in nickel concentration in the remaining liquid during the early stage of coprecipitation was also observed in another group of AAS tests (Figure 3.28). In these tests, the initial Cu: Ni molar ratio was increased to 1:2 to better display the coprecipitation behavior of copper and thus helps identify the precipitation sequence.

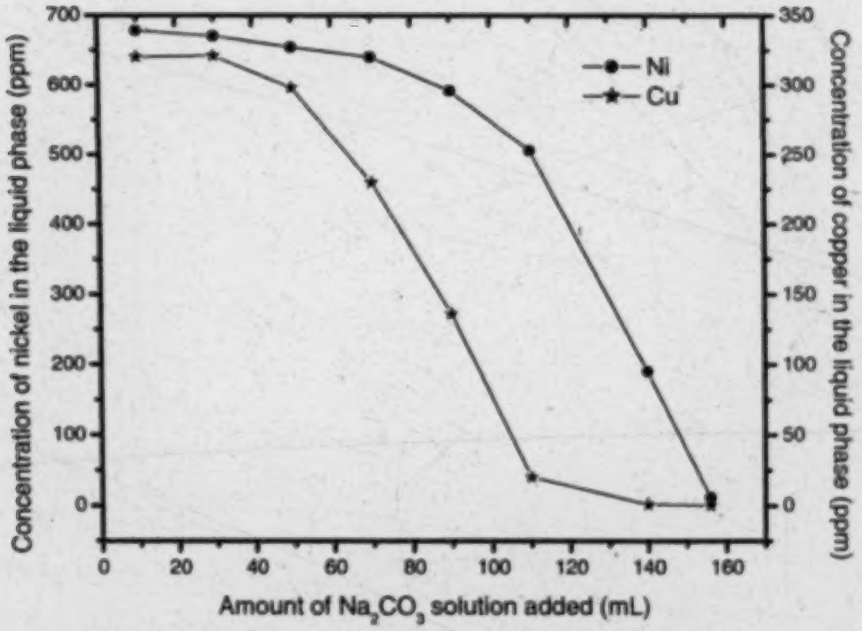

Figure 3.28 Concentration of nickel and copper in the liquid phase with increasing amount of Na_2CO_3 addition. Titration test at T = 95 ℃, V = 200 mL, TMC = 0.2 mol/L and Ni: Al: Cu = 2:1:1 (mole ratio), titrated by 0.25 mol/L Na_2CO_3.

The concentration of copper experienced a sharp decrease when less than 100 mL Na_2CO_3 was added to the solution. However, a slow decrease in the nickel concentration was also observed at this stage of reaction. The results indicate the absence of strict sequential-precipitation. This effect can be attributed to the special coprecipitation nature of copper when HTlcs are supposed to form, that copper cannot form HTlc particles until another type of divalent metal ion is present. Otherwise, the Cu^{2+} cations will form distorted octahedral structures of precipitates, which are energetically preferred to that of HTlc [1].

Furthermore, the total amount of residual nickel and copper in the liquid phase decreases roughly at a constant rate versus the amount of alkali added in the solution after the reaction reached its second plateau. This is consistent with the requirement that the ratio between divalent and trivalent metal ions roughly remains a constant value during the synthesis of HTlcs, no matter how the divalent metal ions precipitate. This result also indicates a coprecipitation process with a constant reaction rate.

3.3.3 Possible Intermediates

As for possible intermediates that may form during the coprecipitation process, Boclair and Braterman [40] speculated that the formation of solid metal hydroxide $M(III)(OH)_3$ contributes to the first plateau. The reaction is given by

$$M(III)^{3+}_{(aq)} + 3(OH)^-_{(aq)} \leftrightarrow M(III)(OH)_3 \qquad (3.4)$$

However, in our experiments solid precipitates were not observed in the first buffer region. It would be more reasonable to speculate the formation of various kinds of intermediate products prior to formation of the metal cations precipitates as hydroxy carbonate HTlc particles. The intermediate products appear in the form of liquid or gel instead of solid.

Several samples were taken during the first buffer region and centrifuged at 30,000 rpm immediately; yet still no solid phase could be observed. Further evidence to support the absence of solid M(III) precipitates in the first buffer region comes from the fact that the concentration of aluminum in the liquid phase of an Al-Ni-Cu system

remained roughly constant throughout the first buffer region, as shown by the AAS results in Figure 3.29.

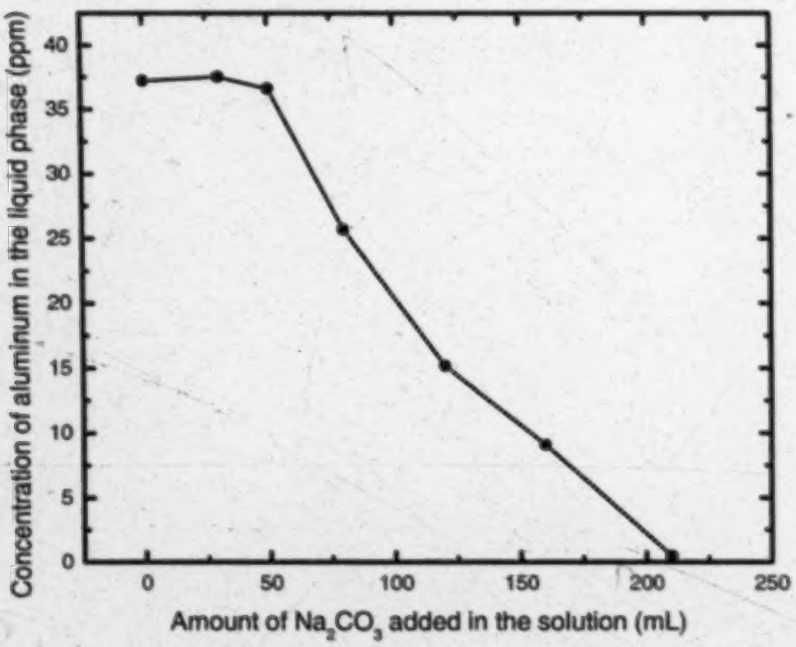

Figure 3.29 Concentration of aluminum in the liquid phase vs. amount of Na_2CO_3 added to the solution. Titration test at T = 95 ℃. V = 100 mL, TMC = 0.2 mol/L, 73% nickel nitrate, 25% aluminum nitrate and 2% copper nitrate, titrated with 0.1 mol/L Na_2CO_3.

A clear plateau could be easily observed when the amount of Na_2CO_3 added to the solution was lower than 50 mL. The presence of the plateau indicates the absence of solid aluminum hydroxide precipitates in this stage of reaction, i.e., solid $Al(OH)_3$ does not form in the first stage of coprecipitation.

In the entire coprecipitation process, assuming that the precipitation of $Al(OH)_3$ is the first step of HTlc formation, it can be calculated that 33.3% of the Na_2CO_3 solution

would be consumed by the end of the first stage of the coprecipitation reaction, to precipitate all the aluminum present. However, only approximately 25% was consumed before the aluminum concentration began to decrease, which further confirm the absence of solid aluminum hydroxide precipitation before nickel and copper join the reaction. An intermediate with the general formula of $Al_n(OH)_{3n-1}^{+}$ would be a more reasonable explanation of what formed during the first stage of the coprecipitation process. The value of "n" could change with time and with the number of anions titrated in or released by urea. As for the plateau of the aluminum concentration in the liquid, Figure 3.30 shows a similar trend line when plotted using bulk pH as the x axis.

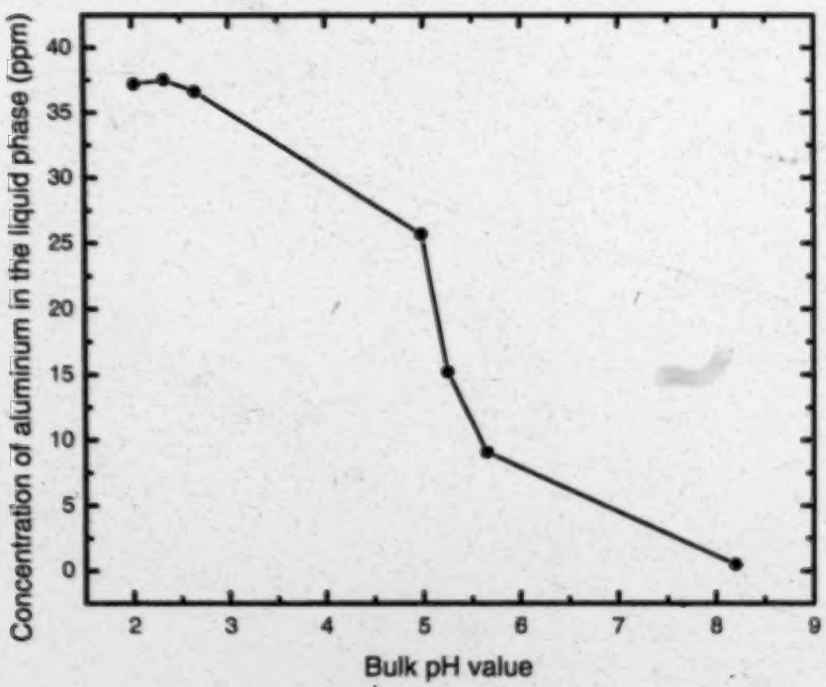

Figure 3.30 Concentration of aluminum in the liquid phase as a function of bulk pH value.

The evolution in aluminum concentration in the liquid could be explained from another angle (concentration of aluminum in the liquid vs. bulk pH value as shown in Figure 3.30). A similar plateau in aluminum concentration could be observed when the bulk pH value was lower than 3.0, which is also roughly the final pH value of the first buffer region in the whole coprecipitation process. This correspondence provides direct proof for the suggestion that solid $Al(OH)_3$ does not form in the first buffer region.

It was also noticed in this work that reaching equilibrium in the second buffer region, or the second plateau of the coprecipitation bulk pH curve, is much slower than that of the first buffer region. Earlier researchers [40] used this effect as an evidence that solid $Al(OH)_3$ forms in early stage of coprecipitation. The reaction rate is anticipated to be slowed when solid reactant is present. It is reasonable to attribute the slow reaction rate to a solid phase reactant being involved in the reaction. However, the "solid phase reactant" is not $M(III)(OH)_3$ precipitates as they speculated [40], but the precipitated hydroxide carbonate HTlc particles. The dominant reaction in the second buffer region of the coprecipitation process is the particle growth reaction in which the previously formed HTlc particles are involved.

To confirm our hypothesis, several samples were selected (Figure 3.31) at different stages of the reaction, the solid part of which was extracted, washed, dried and ground for XRD analysis.

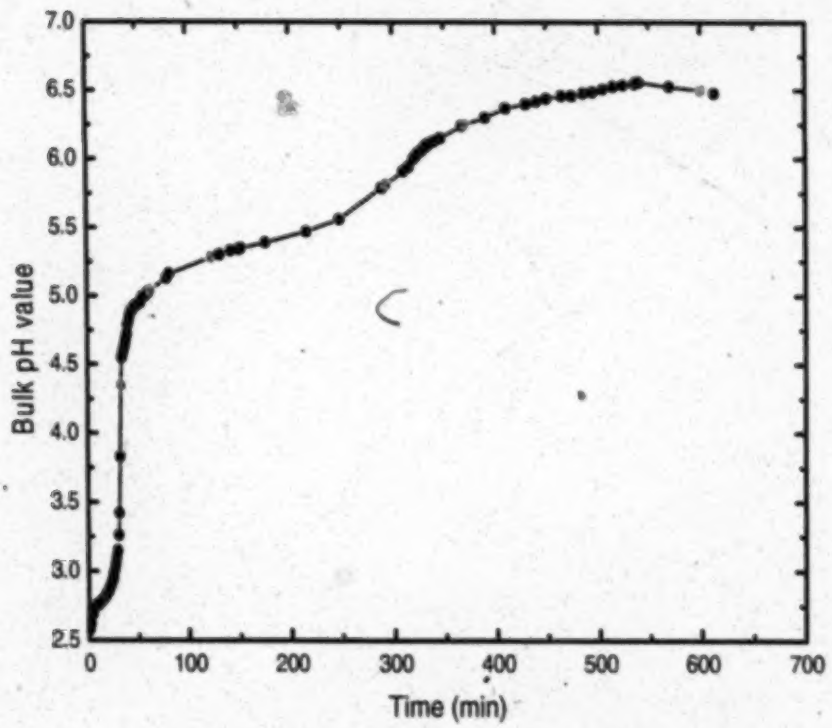

Figure 3.31 XRD samples were taken and prepared for XRD tests at the light points. Coprecipitation using urea with TMC = 0.2 mol/L, PTR = 4.0 and T = 99 ℃.

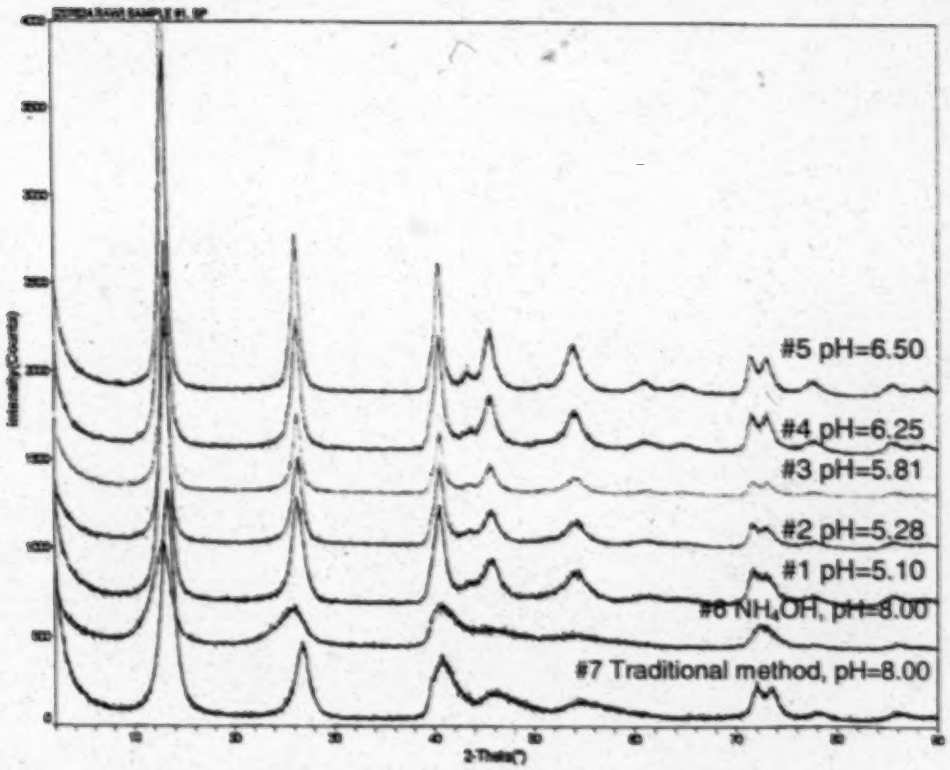

Figure 3.32 XRD patterns of samples at different stages of the coprecipitation process (from sample #1 picked at bulk pH = 5.10 to sample #5 picked at bulk pH = 6.50).

The XRD patterns in Figure 3.32 show that HTlc particles were formed as soon as any solid particles were precipitated from the solution. The slow equilibrium in the second buffer region is attributed to particle growth of solid HTlc particles. This is the dominant reaction in this buffer region especially after the pH reached the second plateau in about 200 minutes. The equilibrium in the second buffer region would be even slower in low relative urea concentration environment where nucleation was further restrained. The XRD patterns of these samples were further compared with the XRD patterns of samples prepared by the traditional constant pH method and samples

prepared by the constant pH method using NH_4OH instead of sodium carbonate and sodium hydroxide as the precipitants, which was unsuccessful.

Adachi-Pagano and his co-workers [41] proposed the formation of certain aluminum aqua-hydroxo complexes, instead of solid aluminum hydroxide in the first buffer region. Rao et al. [42] proposed another hypothetical reaction scheme which includes several intermediates such as $Mg(OH)(H_2O)_x^+$ and $Al(OH)(H_2O)_y^{2+}$.

$$Mg(H_2O)_n^{2+} + H_2O \rightarrow Mg(OH)(H_2O)_{n-1}^+ + H_3O^+ \quad (3.5)$$

$$Al(H_2O)_n^{3+} + H_2O \rightarrow Al(OH)(H_2O)_{n-1}^{2+} + H_3O^+ \quad (3.6)$$

$$Mg(OH)(H_2O)_{n-1}^+ + Al(OH)(H_2O)_{n-1}^{2+} + OH^- + CO_3^{2-} \rightarrow MgAl(OH)_3CO_3 \cdot H_2O + (2n-3)\,H_2O \quad (3.7)$$

The molar ratio between OH^- and Al^{3+} needed to form the intermediate $Al(OH)(H_2O)_{n-1}^{2+}$, as proposed by Rao, was 1:1. However, from the titration experiments, the amount of sodium hydroxide needed to reach the end of the first buffer region is almost the amount needed to form $Al(OH)_3$. This would suggest that in the process of producing HTlc particles using urea hydrolysis, the composition and structure of aluminum-containing intermediate products which would be formed in the first buffer region of the bulk pH value curve would be more complex than that previously proposed. The general reaction could be written as

$$n\,Al(H_2O)_m^{3+} + (3n-1)\,H_2O \rightarrow Al_n(OH)_{3n-1}(H_2O)_{mn-3n+1}^+ + (3n-1)\,H_3O^+ \quad (3.8)$$

3.3.4 Reaction Scheme

The H_3O^+ produced by reaction (3.8) would be compensated by the hydroxides liberated by urea. The number "n" in this reaction, which might be as large as 10, would depend on reaction parameters such as reaction temperature and PTR. In the second buffer region, the divalent metal ions would also form similar intermediate products first, followed by the formation of HTlc particles by reaction with the aluminum-containing intermediate. In an Al-Ni system, the reactions that take place in the second buffer region would be:

$$Ni(H_2O)_n^{2+} + H_2O \rightarrow Ni(OH)(H_2O)_{n-1}^{+} + H_3O^+ \quad (3.9)$$

$$Ni(OH)(H_2O)_{n-1}^{+} + Al_n(OH)_{3n-1}(H_2O)_m^{+} + OH^- + CO_3^{2-} \rightarrow HTlc \quad (3.10)$$

Based on this reaction scheme, the composition of HTlc particles precipitated may vary depending on bulk pH value. Samples taken at a pH value lower than 6.0 (measured at 99 ℃) normally have a low nickel: copper molar ratio in the solid phase. The ratio between divalent metal and trivalent metal may also vary due to different bulk pH values, as the value of "x" in pure nickel-aluminum based HTlc ($[Ni_{1-x}Al_x(OH)_2]^{x+}(A^{n-}_{x/n})\cdot mH_2O$) can vary from 0.20 to 0.33. A mixture of $Al(OH)_3$ and HTlc would form when "x" exceeds 0.33.

A further two experiments were designed to confirm that solid $Al(OH)_3$ does not form in our scheme to form HTlc particles. In the first experiment, solid $Al(OH)_3$ powder was quickly added into a well mixed solution of $Ni(NO_3)_2$ and urea in a 500 mL flask. PTR was set at 4.0, and the liquid mixture was heated to 96℃ under strong magnetic stirring. The product of this experiment was collected after 3 hr

reaction. The mixture in the flask was filtered, washed thoroughly, dried overnight in a vacuum oven and ground for XRD analysis. The XRD patterns are shown in Figure 3.33. The XRD pattern of the sample is more consistent with a mixture of $Al(OH)_3$ and nickel hydroxide hydrate ($Ni(OH)_2 \cdot 0.75H_2O$) instead of showing presence of any HTlc. Most of the peaks, (e.g., the peaks at 21.272°, 23.601°, 42.777°, 43.311°, 44.049°, 45.972°, 48.822°, 59.431°, 61.425°, 64.182°, and 75.685°) fit the XRD pattern of $Al(OH)_3$, and the rest of the peaks, (e.g., the peaks at 13.042°, 26.261°, 40.330° and 72.677°) fit the XRD pattern of $Ni(OH)_2 \cdot 0.75H_2O$ instead of that of HTlc particles.

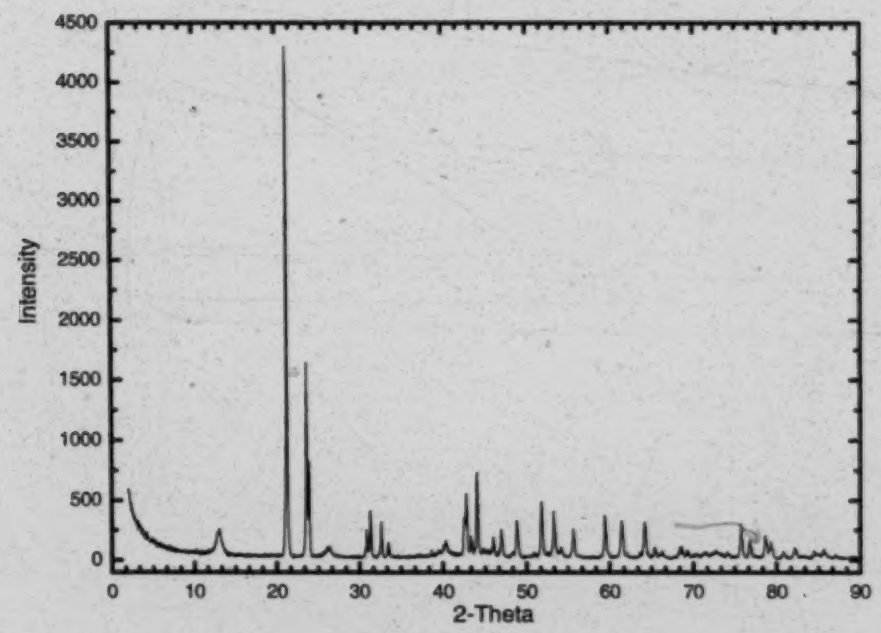

Figure 3.33 XRD pattern. $Al(OH)_{3(solid)} + Ni(NO_3)_2$, PTR = 4.0, T = 96℃, t = 3.0 h.

Should any solid $Al(OH)_3$ forms before HTlc precipitates, the solid $Al(OH)_3$ powder in this experiment should be able to react with the mixture of urea and nickel nitrate

solution, producing HTlc precipitates after even a few minutes. The XRD result proves that no HTlc particles were formed after 3 hr reaction under high temperature and strong stirring condition. Instead, a uniform mixture of aluminum hydroxide hydrate and nickel hydroxide hydrate was found to exist in a large scale. It can be easily concluded from this experiment that solid $Al(OH)_3$ does not possess the capability to react with Ni^{2+} in a matter of minutes in a water phase even at high temperature (96℃). Although we cannot rule out the reaction ($Al(OH)_3 + Ni^{2+}$ --> HTlc) over a much long reaction time ($t > 5$ h), it cannot be what was witnessed during the normal coprecipitation process, in which aluminum hydro-complex as the intermediate product can react with Ni^{2+} in a matter of seconds.

The second experiment provides more direct proof to the suggestion that colloidal aluminum hydro-complex is the principal intermediates for HTlc formation. In this experiment, a mixed solution of aluminum nitrate and urea (without nickel nitrate) was made to PTR = 4.0. The mixture was then heated in a 500mL flask to 96℃ under strong magnetic stir. Colloidal aluminum hydro-complex was found to form after 1 hr of reaction when the bulk pH has reached its second buffer region. Samples were collected after 3 hours reaction. Instead of any $Al(OH)_3$ powder, colloidal aluminum hydro-complex formed by the end of the experiment. It was also noticed that the colloid aluminum starts to form only when the bulk pH reached its second buffer region. Figure 3.34 shows the aluminum hydro-complex colloid.

Figure 3.34 Aluminum hydro-complex colloid. Coprecipitation with PTR = 4.0, TMC = 0.2 mol/L, and T = 99 ℃.

3.4 Formation of Nano-carbon Tubes

Nano-carbon tubes have been used as catalyst supports, as the tip for scanning probe microscopy, and for the storage of hydrogen and many other gases. Many recent papers reported the unique properties of catalytically grown carbon fibers when used as absorbents of hydrocarbons and as catalyst supports [33, 34]. Researchers investigated many other applications, including using the aligned carbon tubes as membrane materials for batteries and fuel cells, anodes for lithium-ion batteries, capacitors and chemical filters. More applications including the usage of carbon nano-tube membranes for electrochemical energy storage and production are still continuously being reported.

It has been regarded as a common conclusion that suitable growth conditions and the properties of the resulting nano-carbon fibers would depend on the chemical nature and physical size of the catalyst particles [52, 53]. As for the growth of nano-carbon tubes from the decomposition of methane, conclusions had been drawn that the length of the nano-carbon tubes increases with the partial pressure of methane and the reaction time. The lengthening rate of the nano-carbon fibers was controlled either by the decomposition of absorbed methane or solid phase carbon diffusion through the metal particle [54, 55]. The lengthening process would end when the catalyst was deactivated.

Iron is regarded as the best catalyst in decomposing methane when heated to a temperature sufficiently high to melt the Fe particles. However, due to the high reaction temperature, the gas phase non-catalytic carbon depositions on the wall of the fiber precede, leading to thickening. This non-catalytic carbon has a completely different structure and lowers the nano-carbon fibers' mechanical properties. Nickel-based catalysts, as an alternative to the Fe catalysts, require much lower decomposition temperatures. The challenge is the easy deactivation of the catalyst [2]. Pure nickel catalyst would be deactivated after just a few seconds of reaction. Compared with the pure nickel catalyst, the catalyst made from Ni-Al based HTlc precursor provides a much longer reaction time while maintaining a high activity and high reaction rate, thus resulting in higher production of nano-carbon fibers. The HTlc precursors would yield a defective, but active nickel phase which has been proposed to be paracrystalline after calcination and reduction [2]. In our experiments, it was found that higher reaction temperature would lead to a higher lengthening rate but a relatively quicker catalyst deactivation, while lower reaction temperature leads to a longer reaction time, but with lower reaction rate.

Nano-carbon tube samples were picked and washed by ultrasonication. The washed samples were analyzed using TEM imaging. The morphology study of the nano-carbon fibers by TEM illustrates that the nano-carbon fibers formed have a curved hollow tubular structure and a diameter range of 18.4 – 59.1 nm. Many dislocations can also be seen from both the internal and the external surface of the tubular structure. These dislocations could greatly increase the surface area and the resistivity to fracture upon deformation. Part of the sample is shown in Figure 3.35.

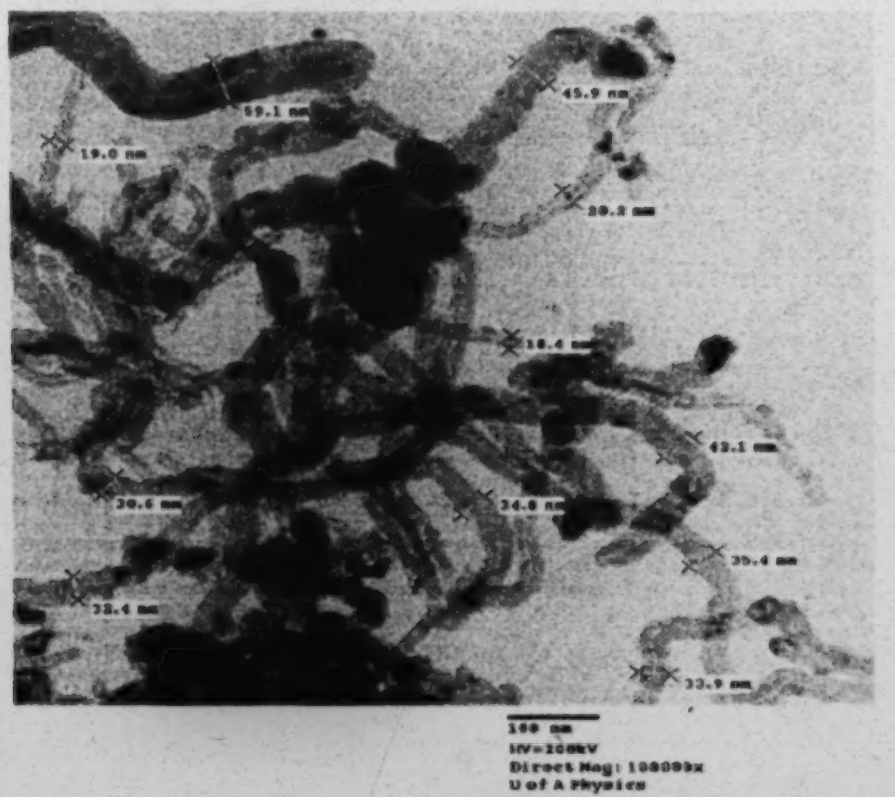

Figure 3.35 TEM micrograph of the nano-carbon tubes formed by decomposing methane. The coprecipitated HTlc catalyst precursor with 75% Ni, 25% Al and 2% Cu was calcined and reduced before used as the final catalyst.

The black dots at the end of most of the nano-carbon tubes are the residual catalyst particles. It could be observed from the TEM micrograph that the diameter of the nano-carbon tubes is almost the same as that of the catalyst particle on the tips of the carbon fibers. Although carbon fibers with uniform diameter have more possible applications, it's difficult to control the size of the catalyst particles which drives the growth. In past years people reported different methods to produce coprecipitated HTlc precursors with highly uniform particle size distribution. However, a number of factors including the calcination temperature, reduction temperature and the composition of the coprecipitated HTlc precursors would affect the average size and the size distribution of the catalyst particles, and thus make it difficult to produce mono-sized catalysts.

Purification of the nano-carbon fibers would be another area of interest. Most of the residue catalyst particles can be removed by ultrasonication, the rest of which may require special process as etching, benzene-HCl washing, ultrasonication-assisted filtration, freezing treatment [56] and the use of magnetic field to achieve a complete removal. TEM micrograph of the nano-carbon tube samples after ultrasonication could be seen in Figure 3.36. Residual catalysts could be seen in the picture as black dots.

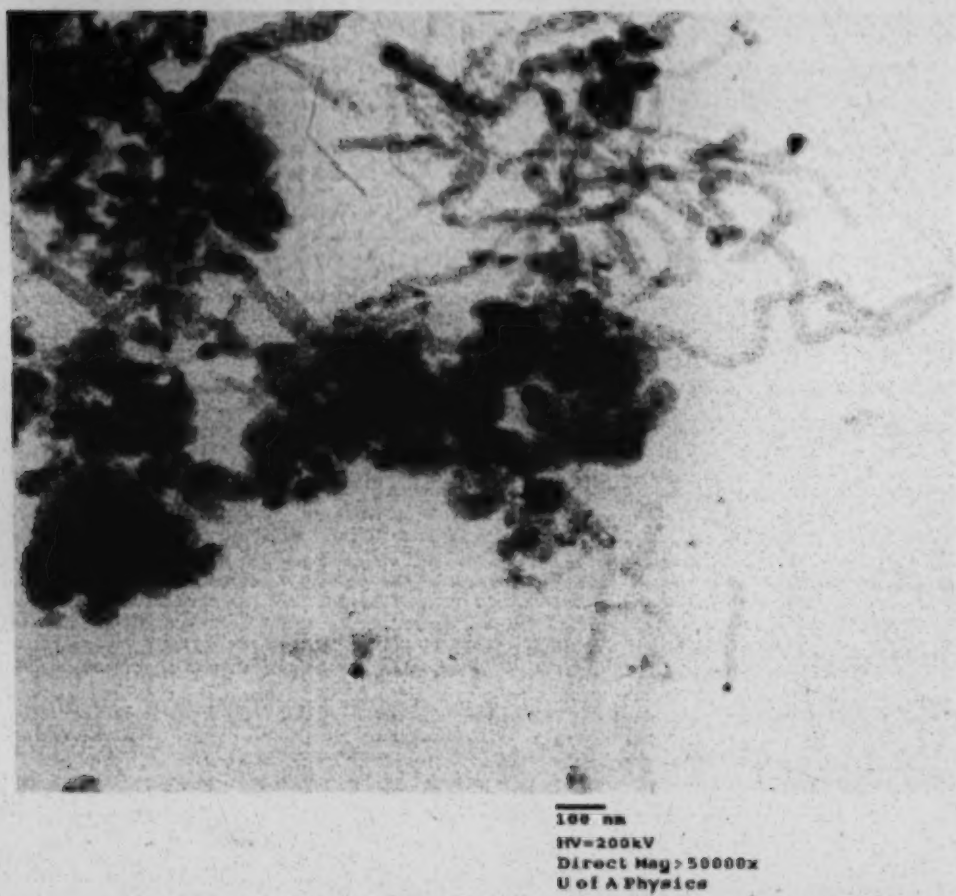

Figure 3.36 TEM micrograph of another part of the nano-carbon tubes formed by decomposing methane. Clumps of catalysts (black dots) can be seen in this picture.

4 Conclusions

HTlcs were synthesized using the urea coprecipitation method. Different PTR (relative urea concentration) were used in several groups of tests. Samples were taken and particle sizes were analyzed by Malvern SM2000 Master-Sizer® and XRD.

It is found that low PTR usually gives rise to precipitates with large average particle size. This is because under low supersaturation conditions nucleation is rare while particle growth is the dominant reaction in the whole coprecipitation process. XRD results confirmed the speculation. The average particle size would decrease as PTR increases from 1.0 to 4.0, reaching its minimum value at PTR = 4.0, then increase again with PTR when PTR is larger than 4.0. This effect is attributed to the extensive agglomeration among the precipitated particles. In the high supersaturation conditions where the rate of nucleation can be much higher than the rate of particle growth, smaller particles are supposed to form, but agglomerate at later stages of the coprecipitation process. Calculations based on XRD results confirmed this conjecture.

Samples were also examined by SEM. "Sand rose" morphology which indicates extensive agglomeration among the precipitates were found to be prevalent in the samples prepared by urea coprecipitation method. Better control of reaction temperature and PTR might help solve the problem.

In an Al-Cu-Ni system, two distinct buffer regions were found to occur in the bulk pH curve of the coprecipitation process. The pH value of the first buffer region is controlled by the trivalent metal ions, aluminum in this case, present in the solution.

The position of the first buffer region has no relationship with the divalent metal ions. However, the length of the first buffer region is controlled by multiple parameters including the reaction temperature and mole ratio of metal cations and anions (OH^- and CO_3^{2-}).

Moreover, different divalent metal ions present in the solution were found to precipitate following a certain sequence. In the Al-Cu-Ni system studied in this work, copper precipitates earlier than nickel. The AAS results show a sharp increase in the ratio of nickel to copper concentration in the liquid phase when coprecipitation starts, indicating that much more copper precipitates before nickel does. However, there is no strict precipitation sequence. A certain amount of nickel joins in the coprecipitation before all the copper becomes precipitated. This effect is attributed to the special coprecipitation property of copper. Copper would not be able to form HTlc particles unless another divalent metal is present.

An aluminum hydro-complex written as $Al_n(OH)_{3n-1}(H_2O)_m^+$, instead of solid $Al(OH)_3$ or $Al(OH)(H_2O)_n^{2+}$ as suggested by earlier researchers was found to be the intermediate product before HTlc formation. AAS results shows that the aluminum concentration in the liquid did not decrease throughout the first buffer region, indicating the absence of solid $Al(OH)_3$ precipitates during this stage of reaction. XRD results prove that HTlc forms as soon as any solid particles form, while no solid would form before that. The slow equilibrium in the second buffer region of the coprecipitation process is attributed to the presence of solid HTlc as a main reactant in that stage of reaction, when particle growth is supposed to be the dominant reaction.

A new tentative coprecipitation reaction scheme for Al-Ni system is advanced. The new reaction scheme could be written as follows:

$$n\ Al(H_2O)_m^{3+} + (3n-1)\ H_2O \rightarrow Al_n(OH)_{3n-1}(H_2O)_{mn-3n+1}^{+} + (3n-1)\ H_3O^{+} \quad (4.1)$$

$$Ni(H_2O)_n^{2+} + H_2O \rightarrow Ni(OH)(H_2O)_{n-1}^{+} + H_3O^{+} \quad (4.2)$$

$$Ni(OH)(H_2O)_{n-1}^{+} + Al_n(OH)_{3n-1}(H_2O)_m^{+} + OH^{-} + CO_3^{2-} \rightarrow HTlc \quad (4.3)$$

5 Suggestions for Future Work

Since the "sand rose" morphology would lead to a very low specific surface area with nearly no porosity [41] and the aggregates are quite resistant to dispersion (remain aggregated even under powerful ultrasonic treatments), it is necessary to eliminate the presence of the "sand rose" morphology. Various reaction temperature and PTR are worth trying to optimize coprecipitation conditions for the synthesis of Cu-Ni-Al based HTlcs. In order to obtain small size precipitates, a PTR = 4.0 with high reaction temperature is suggested. However the overlap of particle growth and agglomeration gives rise to a relatively wide particle size distribution. More work is needed to identify conditions suitable for synthesizing uniform particles.

As certain precipitation sequence exists in the coprecipitation process, the composition of the precipitated HTlc particles may change with reaction time. In a Ni-Al-Cu system, samples picked at different stages of the reaction can have different Ni: Cu ratio, which may affect the catalytic activity of the final catalysts. However, this effect could also be utilized to obtain HTlc particles with certain ratios among multiple divalent metals, e.g. Ni: Cu ratio in the Ni-Al-Cu system. More work is needed to achieve better control of the composition and ratios between different metal cations in the precipitates.

In addition to the Ni-Al-Cu system discussed in this work, Ni-Fe-Cu and Ni-Fe systems are also interesting to study. As iron has higher activity than aluminum when acting as hydrogenation catalyst, more attention should be paid to the Ni-Fe-Cu or Ni-Fe based HTlc catalyst precursors.

Nomenclature

The following nomenclature will be used in the remainder of this work:

HT = Hydrotalcite = $Mg_6Al_2(OH)_{16}CO_3 \cdot 4H_2O$

HTlc = Hydrotalcite-like compound = $M(II)_{1-z}M(III)_z(OH)_2)(X_{z/2}) \cdot y\,H_2O$ (X = e.g., CO_3^{2-})

PTR = Practical-Theoretical Ratio = the ratio between the amount of urea that was used in the experiment and the stoichiometric value.

TMC = Total Metal salts Concentration = $[Ni^{2+}] + [Al^{3+}] + [Cu^{2+}]$

References

1. Cavani, F.; Trifiro, F.; Vaccari, A. *Catalysis Today*, 1991, 11, 173-301.
2. Heidi M. Jensen, PhD degree thesis, University of Oslo, 2003
3. Li, Y; Chen, J; Chang, L. *Appl. Catal.* A 1997, 163, 45-57.
4. Armor, J. N. *Appl. Catal.* A 1999, 176, 159-76.
5. Andrews, L. D. *J. Power Sources* 1996, 61, 113-24.
6. Steinberg, M.; Cheng H. C. *Int. J Hydrogen Energy* 1989, 14, 797-820.
7. Muradov, N. Z. *Int. J. Hydrogen Energy*, 1993, 18, 211-15.
8. Muradov, N. Z. *Energy Fuels* 1998, 12, 41-48.
9. Muradov, N. Z. *Prepr. Pap. – Am Chem. Soc. Div. Fuel Chem.* 2001, 46(1), 29-30.
10. Bromberg, L.; Cohn, D. R.; Rabinovich, A.; Alexeev, N. *Prepr. Pap – Am Chem. Soc., Div. Fuel Chem.* 2001, 46(1), 1-4.
11. Bromberg, L.; Cohn, D. R.; Rabinovich, A.; Alexeev, N. *Int. J. Hydrogen Energy* 1999, 24, 1131-37,125
12. Rabinovich, A.; Cohn, D. R.; Bromberg, L. U.S. Patent 5,437,250, August 1, 1995.
13. Dahl, J. K.; Tamburini, J.; Weimer, A. W.; Lewandowski, A. Pitts, R.; Bingham, C.; Glatzmaier, G. C. *Prepr. Pap. – Am. Chem. Soc., Div. Fuel Chem.* 2001, 46(1), 22-26.
14. Kurosaka, T.; Matsuhashi, H.; Arata, K. *J. Catal.* 1998, 179, 28-35.
15. Zhang, T.; Amiridis, M. D. *Appl. Catal. A: General* 1998, 167, 161-72.
16. Kuvshinov, G. G.; Mogilynkh, Y. I.; Kuvshinov, D. G. *Catal. Today* 1998, 42, 357-60.
17. Ermakova, M. A.; Ermakov, D. Y.; Kuvshinov, G. G. *Appl. Catal. A: General* 2000, 201, 61-70.
18. Li, Y.; Chen. J.; Qin, Y.; Chang, L. *Energy Fuels* 2000, 14, 1188-94.
19. Gao, X. P.; Qin, X.; Wu, F.; Liu, H.; Lan, Y.; Fan, S. S.; Yuan, H. T.; Song, D. Y.; Shen, P. W. *Chem. Phys. Lett.* 2000, 327, 271-76.
20. Choudhary, T.V.; Sivadinarayana, C.; Chusuei, C. C.; Klinghoffer, A.; Goodman, D. W. *J. Catal.* 2001, 199, 9-18.
21. Otsuka, K.; Seino, T.; Kobayashi, S.; Takenaka, S. Chem. Lett. 1999, 11, 1179-80.

22. Otsuka, K.; Kobayashi, S.; Takenaka, *S. Appl. Catal. A: General* 2000, 190, 261-68.

23. Otsuka, K.; Kobayashi, S.; Takenaka, *S. Appl. Catal. A: General* 2001, 210, 371-79.

24. Otsuka, K.; Mito, A.; Takenaka, S.; Yamanaka, I. *Int. J. Hydrogen Energy* 2001, 26, 191-94.

25. Saito, Y. *Carbon* 1995, 33, 979-88.

26. Li, W. Z.; Xie, S. S.; Qian, L. X.; Chang, B. H.; Zou, B. S.; Zhou, W. Y.; Zhao, R. A.; Wang, G. *Science* 1996, 274, 1701-03.

27. Journet, C.; Maser, W. K.; Bernier, P.; Louiseau, A.; Lamy de la Chapelle, M.; Lefrant, S.; Deniard, P.; Lee, R.; Fischer, J. E. *Nature* 1997, 388, 765-68.

28. Rodriguez, N. M. *J. Mater. Res.* 1993, 8, 3233-50.

29. Chen, P.; Zhang, H. B.; Lin, G. D.; Hong, Q.; Tsai, K. R. *Carbon* 1997, 35, 1495-1501.

30. Avdeeva, L. B.; Goncharova, O. V.; Kochubey, D. I.; Zaikovskii, V. I.; Plyasova, L. M.; Novgorodov, B. N.; Shaikhutdinov, S. K. *Appl. Catal.* A 1996, 141, 117-29.

31. Fenelonov, V. B.; Derevyankin, A. Y.; Okkel, L. G.; Avdeeva, L. B.; Zeikovskii, V. I.; Moroz, E. M.; Salanov, A. N.; Rudina, N. A.; Likholobov, V. A.; Shaikhutdinov, Sh. K. *Carbon* 1997, 35, 1129-40.

32. Nolan, P. E.; Lynch, D. C.; Culter, A. H. *Carbon* 1994, 32, 477-83.

33. V. B. Fenelonov; L. B. Avdeeva; O. V. Goncharova; L. G. Okkel; P. A. Simonov; A. Y. Derevyankin; V. A. Likholobov. *Stud. Surf. Sci. Cat. Preparation of Catalyst* VI, 91 (1995) 825.

34. M. S. Kim; N. M. Rodriguez; R. T. K. Baker. *Synthesis and Properties of Advanced Catalytic Materials, Materials Research Society Symposium Proceedings.* Materials Research Society, Pittsburgh, PA, USA, 1995, 368, 99-104.

35. Kruissink, E. C.; Pelt, H. L.; Ross, J. R. H.; Van Reijen, L. L. *Appl. Catal.* 1981, 1, 23-29.

36. Narita, E.; Matsuno, Y.; Takahashi, S.; Umetsu, Y. *J. Chem. Soc. Jpn.* 2001, 5, 273.

37. Costantino, U.; Marmottini, F.; Nochetti, M.; Vivani, R. *Eur. J. Inorg. Chem.* 1998, 1439.

38. Cai, H.; Hillier, A. C.; Franklin, K. R.; Nunn, C. C.; Ward, M. D. *Science*, 1994, 266, 1551.

39. Costantino, U.; Coletti, N.; Nocchetti, M.; Aloisi, G. G.; Elisei, F.; Latterini, L. *Langmuir*, 2000, 16, 10351.

40. Boclair, J. W.; Braterman, P. S. *Chem. Mater.* 1999, 11, 298-302.

41. Adachi-Pagano, M; Forano, C.; Besse, J. *J. Mater. Chem.*, 2003, 13, 1988-93

42. Rao, M. M.; Reddy, B. R.; Jayalakshmi, M.; Jaya, V. S.; Sridhar, B. *Materials Research Bulletin*, 2005, 40, 347-59.

43. F. E. Shephard. *J. Catal.*, 1969, 14, 148.

44. V. A. Dzis'ko; S. P. Noskova; M. S. Borisova; V. D. Bolgova; L. G. Karakhciev. Kinet. *Catal. (Engl. Transl.)*, 1974, 15, 667.

45. M. S. Borisova; V. A. Dzis'ko; L. G. Simonova. Kinet. *Catal. (Engl. Transl.)*, 1974, 15, 425.

46. F. Iosht; A. L. Klyachko-Gurvich; A. M. Rubinstein. Izr. Akad. Nauk. *SSSR. (Engl. Transl.)*, 1963, 1942.

47. Luis E. Alzamora; Julian R. H. Ross; Edgar C. Kruissink; Louis L. Van Reijen. *J. Chem. Soc., Faraday Trans*, 1, 1981, 77, 665-81.

48. Huang, C. P.; Richardson, J. *T. J. Catal.*, 1978, 51, 1.

49. Naghash, A. R.; Xu, Z.; Etsell, T. H. *Chemistry of Materials*, 2005/Vol 17, Iss. 4 815-21.

50. Puxley, D. C.; Kitchener, I. J.; Komodromos, C.; Purkgns, N. D. *Stud. Surf. Sci. Catal.* 1983, 16, 227.

51. Li, Y. D.; Chen, J. L.; Chang, L.; Qin, Y. N. J. Catal. 1998, 178, 76-83.

52. Benissad, F.; Gadelle, P.; Coulon, M.; Bonnetain, L. *Carbon* 1988, 26, 61.

53. Benissad, F.; Gadelle, P.; Coulon, M.; Bonnetain, L. *Carbon* 1989, 27, 585.

54. Kim, M. S.; Rodriguez, N. M.; Baker, R. T. K. *J. Catal.* 1992, 134, 253.

55. Bianchini, E. C.; Lund, C. R. F. *J. Catal.* 1989, 117, 455.

56. Li. F; Cheng, H. M.; Xing, Y. T.; Tan, P. H.; Su, G. *Carbon* 2000, 38, 2041-45.

57. Ogawa, M.; Kaiho H. *Langmuir* 2002, 18, 4240-42.

58. Shaw, W. G. R.; Bordeaux, J. J. *J. Am. Chem. Soc.* 1955, 77, 4729.

59. Malherbe, F.; Forano, C.; Besse, J. P. *Microporous Mater.* 1997, 10, 67.